RECLAMATION

Managing Water in the West

Hydraulic Laboratory Report HL-2011-09

Physical Hydraulic Modeling of Canal Breaches

U.S. Department of the Interior
Bureau of Reclamation
Technical Service Center
Hydraulic Investigations and Laboratory Services Group
Denver, Colorado

September 2011

REPORT DOCUMENTATION PAGE

Form Approved
OMB No. 0704-0188

The public reporting burden for this collection of information is estimated to average 1 hour per response, including the time for reviewing instructions, searching existing data sources, gathering and maintaining the data needed, and completing and reviewing the collection of information. Send comments regarding this burden estimate or any other aspect of this collection of information, including suggestions for reducing the burden, to Department of Defense, Washington Headquarters Services, Directorate for Information Operations and Reports (0704-0188), 1215 Jefferson Davis Highway, Suite 1204, Arlington, VA 22202-4302. Respondents should be aware that notwithstanding any other provision of law, no person shall be subject to any penalty for failing to comply with a collection of information if it does not display a currently valid OMB control number.

PLEASE DO NOT RETURN YOUR FORM TO THE ABOVE ADDRESS.

1. REPORT DATE *(DD-MM-YYYY)*	**2. REPORT TYPE**	**3. DATES COVERED** *(From - To)*
20-09-2011	Technical	October 2009 – September 2011

4. TITLE AND SUBTITLE	**5a. CONTRACT NUMBER**
Physical Hydraulic Modeling of Canal Breaches	**5b. GRANT NUMBER**
	5c. PROGRAM ELEMENT NUMBER
6. AUTHOR(S)	**5d. PROJECT NUMBER** 8442
Tony L. Wahl, Dale J. Lentz	**5e. TASK NUMBER**
	5f. WORK UNIT NUMBER

7. PERFORMING ORGANIZATION NAME(S) AND ADDRESS(ES)	**8. PERFORMING ORGANIZATION REPORT NUMBER**
U.S. Dept. of the Interior, Bureau of Reclamation Technical Service Center, 86-68460 Denver, CO 80225	**HL-2011-09**
9. SPONSORING/MONITORING AGENCY NAME(S) AND ADDRESS(ES)	**10. SPONSOR/MONITOR'S ACRONYM(S)**
U.S. Department of the Interior, Bureau of Reclamation Research and Development Office, 86-69000 P.O. Box 25007 Denver, CO 80225	**11. SPONSOR/MONITOR'S REPORT NUMBER(S)**

12. DISTRIBUTION/AVAILABILITY STATEMENT
National Technical Information Service, 5285 Port Royal Road, Springfield, VA 22161
http://www.ntis.gov

13. SUPPLEMENTARY NOTES

14. ABSTRACT

Canals have the potential to be a source of serious flooding when embankments erode and breach. To assess and address risks associated with canal embankments, the erosion and breach processes must be understood so that potential flooding can be modeled. Breaching processes for canal embankments are potentially different from those of traditional embankment dams impounding large reservoirs due to several factors, including the effect of water flowing in a canal past the developing breach and limitations on the ability of a canal to convey water to a breach site as the breach develops. This may significantly affect the mechanics of the erosion process and the resulting breach outflow hydrograph. This study used laboratory physical models to study the breaching processes of typical canal embankments. The effects of varying material properties and different failure initiation conditions were considered. Material erodibility was quantified by in situ and laboratory submerged jet erosion testing. Relations for predicting canal breach outflow rates as a function of canal and embankment geometry and geotechnical/erodibility characteristics are proposed. These relations could support appraisal-level evaluation of flooding risks posed by existing canals. For detailed analyses of specific cases, the data collected in this study can support the development of canal-specific breach simulation computer models.

15. SUBJECT TERMS
Canal, levee, safety, erosion, erodibility, dam failure, internal erosion, piping, overtopping flow, breach development, flood modeling, physical hydraulic modeling.

16. SECURITY CLASSIFICATION OF:			**17. LIMITATION OF ABSTRACT**	**18. NUMBER OF PAGES**	**19a. NAME OF RESPONSIBLE PERSON**
			SAR	56	Robert F. Einhellig
REPORT	**ABSTRACT**	**THIS PAGE**			**19b. TELEPHONE NUMBER** *(Include area code)*
UU	UU	UU			303-445-2142

Standard Form 298 (Rev. 8/98)
Prescribed by ANSI Std. Z39.18

Hydraulic Laboratory Report HL-2011-09

Physical Hydraulic Modeling of Canal Breaches

Prepared by:

Tony L. Wahl, P.E.
Hydraulic Engineer, Hydraulic Investigations and Laboratory Services Group, 86-68460

Dale J. Lentz, P.E.
Hydraulic Engineer, Hydraulic Investigations and Laboratory Services Group, 86-68460

Technical Approval:

Robert F. Einhellig, P.E.
Manager, Hydraulic Investigations and Laboratory Services Group, 86-68460

Peer Review:

Bruce D. Feinberg, P.E.
Hydraulic Engineer, Flood Hydrology and Emergency Management Group, 86-68250

9/20/11
Date

U.S. Department of the Interior
Bureau of Reclamation
Technical Service Center
Hydraulic Investigations and Laboratory Services Group
Denver, Colorado

September 2011

Mission Statements

The mission of the Department of the Interior is to protect and provide access to our Nation's natural and cultural heritage and honor our trust responsibilities to Indian Tribes and our commitments to island communities.

The mission of the Bureau of Reclamation is to manage, develop, and protect water and related resources in an environmentally and economically sound manner in the interest of the American public.

Acknowledgments

The hydraulic model test facility and the tested embankments were constructed by the hydraulics laboratory shop staff, specifically carpenters Jason Black, Jimmy Hastings, and Marty Poos, and machinist Dane Cheek. Measurements of in situ soil density were made by Bobby Rinehart and Caleb Rudkin of the Materials Engineering Research Laboratory. Staff of the Lower Colorado Regional Office supported the work and contributed to the development of the project test plan, including Scott Foster, Nathaniel Gee, and Doug Blatchford. Bruce Feinberg of Reclamation's Flood Hydrology and Emergency Management Group identified the first need for this study and provided peer review of this report. Jeff Farrar, Chris Slaven, Dave Edwards, and Perry Hensley also provided advice and review comments during the course of the study.

Hydraulic Laboratory Reports

The Hydraulic Laboratory Report series is produced by the Bureau of Reclamation's Hydraulic Investigations and Laboratory Services Group (Mail Code 86-68460), PO Box 25007, Denver, Colorado 80225-0007. At the time of publication, this report was also made available online at **http://www.usbr.gov/pmts/hydraulics_lab/pubs/**.

Disclaimer

The information provided in this report is believed to be appropriate and accurate for the specific purposes described herein, but users bear all responsibility for exercising sound engineering judgment in its application, especially to situations different from those studied. References to commercial products do not imply endorsement by the Bureau of Reclamation and may not be used for advertising or promotional purposes.

This work was funded by Reclamation's Research and Development Office, project number 8442.

CONTENTS

EXECUTIVE SUMMARY 1

INTRODUCTION AND PURPOSE 2

BACKGROUND AND LITERATURE REVIEW 2
- Canals and Levees 3
- Modeling Embankment Erosion Processes 4
- Comparing Dams, Levees, and Canals 5
- Canal Breach Studies 6

MODEL CONSIDERATIONS 7
- Model Scaling Laws 8
  - Scaling Material Properties 8
- Canal Dynamics 9

MODEL DESCRIPTION 10
- Test Facility 10
- Embankment Materials 12
  - Soil Selection and Testing 13

EMBANKMENT PLACEMENT AND TESTING 14
- Test Procedures 15
- Embankment 1 16
- Embankment 2 21
- Embankment 3 24

DISCUSSION 27
- Erosion Rates 29
- Breach Initiation Process 31
  - Piping Erosion 32
  - Headcut Advance 33
- Comparison to Embankment Dam Breaches 35

EFFECTS OF CANAL HYDRODYNAMICS 35
- HEC-RAS Modeling 38

APPRAISAL-LEVEL ESTIMATES OF CANAL BREACH HYDROGRAPHS 47
- Breach Initiation 47
  - Breach Initiation by Headcut Advance due to Overtopping Flow 48
  - Breach Initiation by Headcut Advance due to Piping Flow 49
  - Breach Initiation by Pipe Enlargement 50
- Breach Development 51

CONCLUSIONS 53

REFERENCES 54

TABLES

Table 1. — Characteristics of dams, levees and canals relevant to breach modeling. 5

Table 2. — Soil characterization. 13

Table 3. — Breach initiation and development times from model embankment tests. Prototype values in parentheses are representative times for a prototype that is 16 times larger than the tested model. 27

Table 4. — Erosion rates during embankment breach tests..... 29

Table 5. — Comparison of observed breach widening rates and those predicted using relation by Hunt et al. (2005). 30

Table 6. — Characteristics of breach outflow hydrographs for HEC-RAS simulations of the breach of the example canal..... 44

Table 7. — Approximate values of k_d in cm^3/(N-s) as a function of compaction conditions and % clay (Hanson et al. 2010). [1 cm^3/(N-s) = 0.5655 ft/hr/psf]..... 49

Table 8. — Approximate values of τ_c in Pa as a function of compaction conditions and % clay (Hanson et al. 2010). [1 Pa = 0.0209 psf] 49

Table 9. — Approximate values of τ_c in Pa as a function of compaction conditions and %clay (modified from Hanson et al. 2010). These values of τ_c are representative of submerged jet test results. For use in the piping erosion model (Eq. 10), they should be increased by a factor of 100. [1 Pa = 0.0209 psf] 51

FIGURES

Figure 1. — Overview of the breach of the Truckee Canal near Fernley, Nevada, January 5, 2008..... 4

Figure 2. — Breach of the Bridgewater Canal, 1971. Note three people standing in the center of the breach and the large headcut that has retreated up the far reach of the canal. (Photo courtesy of Bridgewater Canal Company.)..... 7

Figure 3. — Plan view of canal breach model test facility. Flow enters via the head boxes at each end of the model. 10

Figure 4. — Cross-section view of model canal and embankment test section. 11

Figure 5. — Changes in dry unit weight, γ_d, and detachment rate coefficient, k_d, as a function of water content for standard Proctor compaction test specimens. 14

Figure 6. — Electric jackhammer fitted with custom compaction plate. 16

Figure 7. — Performing sand cone density test at the halfway point of embankment construction. 17

Figure 8. — Performing *in situ* submerged jet erosion test. 17

Figure 9. — Embankment 1 prior to breach testing..... 19

Figure 10. — Headcut migration rate into embankment 1. These data were obtained by physically probing for the headcut face and measuring its distance from a downstream reference point during the test..... 19

Figure 11. — Breach widening during testing of embankment 1..... 20

Figure 12. — Post-test measurement of soil erodibility using the submerged jet test..... 20

Figure 13. — Flow hydrographs and water levels from breach test of embankment 1..... 21

Figure 14. — Embankment 2 under construction. Remnants of embankment 1 are marked by white paint lines at the edges. 22

Figure 15. — Flow hydrographs and water levels from breach test of embankment 2..... 23

Figure 16. — Headcut and breach widths during the testing of embankment 2..... 24

Figure 17. — Headcut advance through embankment 3 during the breach initiation phase. Labels are elapsed time in hours and minutes. Horizontal position of headcuts was determined by physically probing from downstream side of embankment. Headcut heights are estimated. 25

Figure 18. — Headcut and breach widening rate during breach of embankment 3. Breach widening rate during breach development phase (approximately 4:48 to 4:56) was 0.64 ft/min..... 26

Figure 19. — Location of headcut advancing up the invert of the west (downstream) canal following breach of canal embankment. Distances are from the centerline of the breach opening. Headcut advance rate was 0.77 ft/min. 26

Figure 20. — Water levels and flow rates during test of embankment 3. 27

Figure 21. — Soil compaction and erodibility properties of test embankments compared to standard Proctor compaction test results..... 28

Figure 22. — Erodibility parameters of tested model canal embankments (filled symbols) and values adjusted to represent a hypothetical prototype 16 times larger than the tested model

(open symbols). Erodibility classification boundaries are those proposed by Hanson and Simon (2001). 29

Figure 23. — Relation between headcut advance rate coefficients and soil detachment rate coefficients. Data points represent the range of pre-and post-test jet erosion test results for each embankment..... 34

Figure 24. — Example water surface profiles computed for upstream canal following canal breach. 38

Figure 25. —HEC-RAS simulation of 6 min breach of example canal embankment with 2 miles distance to nearest upstream and downstream check structures. In (a), initial canal flow is from right to left. 41

Figure 26. —HEC-RAS simulation of 6 min breach of example canal embankment with 50 miles distance to nearest upstream and downstream check structures. In (a), initial canal flow is from right to left. 42

Figure 27. —Differences in simulated breach outflow for breach development times of (a) 2 hr and (b) 1 min. The breaches are located at the midpoint of a 4-mile long canal reach between two check structures with a 3,000 ft^3/s constant inflow boundary condition at the upstream end and a normal depth boundary condition at the downstream end. 43

Figure 28. — Dimensionless peak discharge as a function of dimensionless breach development time. 45

Figure 29. — Effect of downstream canal reach length on peak breach outflow. 46

Figure 30. — Hydrograph recession time as a function of breach development time..... 47

Figure 31. — Canal embankment parameters for estimating headcut advance rate due to overtopping flow. 48

Figure 32. — Canal embankment parameters for estimating headcut advance rate due to piping flow. 49

GLOSSARY OF SYMBOLS

A	cross-sectional area
A_1	cross-sectional area upstream from critical section
A_c	cross-sectional area at critical depth
b_{max}	final breach width
C	headcut advance rate coefficient, $s^{1/3}$/hr
D	hydraulic depth, A/T
d_{pipe}	piping hole diameter
dW/dt	rate of breach width enlargement
dX/dt	rate of headcut advance
E	specific energy
Fr	Froude number
f	Darcy friction factor
g	acceleration due to gravity, 32.2 ft/s^2
H_1	total energy head upstream from critical section
H_h	headcut height
H_{ov}	overtopping head
H_{pipe}	net head on piping hole
h_1	gaged flow depth upstream from critical section
k_d	detachment rate coefficient, (ft/hr)/(lb/ft^2), or ft/hr/psf
$k_{d,r}$	model-prototype detachment rate coefficient ratio
L	headcut advance distance to initiate breach failure
L_{ds}	downstream canal reach length
L^*_{ds}	dimensionless downstream canal reach length
L_{pipe}	length of piping hole
L_r	model-prototype length ratio
L_{us}	upstream canal reach length
L^*_{us}	dimensionless upstream canal reach length
n	Manning's n roughness coefficient, dimensionless
Q	discharge (flow rate)
Q_0	discharge through piping hole at time t=0
$Q_{c,max}$	maximum theoretically possible breach outflow
$Q^*_{envelope}$	upper envelope of dimensionless peak outflow rates
Q_{normal}	design discharge of canal at normal-depth conditions
Q_{peak}	peak outflow rate from canal breach
Q^*_{peak}	dimensionless peak outflow rate from canal breach
Q_r	model-prototype discharge ratio
$Q(t)$	flow rate through piping hole at time t
q	discharge per unit width
R_h	hydraulic radius
S	hydraulic gradient, dimensionless
T	channel top width
T_c	channel top width at critical depth
t	time
t_{er}	piping erosion time scale

t_f	breach development time
t^*_f	dimensionless breach development time
$t_{initiation}$	breach initiation time
t_r	model-prototype time ratio
$t_{recession}$	breach hydrograph recession time
$t^*_{recession}$	dimensionless breach hydrograph recession time
t_{ref}	breach development reference time
V	flow velocity
V_r	model-prototype velocity ratio
y_c	critical depth
y_n	normal depth
γ_d	dry unit weight
γ_w	unit weight of water, 62.4 lb/ft^3
$\dot{\varepsilon}$	volumetric erosion rate, ft^3/ft^2/hr, which simplifies to ft/hr
τ	applied shear stress
τ_c	critical shear stress needed to initiate sediment detachment
τ_{ew}	effective stress on breach sidewalls
τ_0	initial shear stress inside piping hole at time t=0

Executive Summary

This research report provides a comprehensive evaluation of issues related to the modeling of potential canal embankment breaches and the determination of associated breach outflow hydrographs. A combination of physical model tests and numerical modeling was used to investigate different failure initiation conditions, the erodibility characteristics of embankment soils, and canal hydrodynamic effects that constrain peak breach outflow rates. Analyzing different erosion phases within the physical model tests, there was good correlation between the model tests and similar studies performed at other laboratories on traditional embankment dams.

Appraisal-level procedures were developed for estimating the temporal and geometric properties of canal breaches and associated outflow hydrographs. The procedures can make use of either measured soil erodibility parameters (field or lab) or estimated parameters derived from other basic soil properties and knowledge of original embankment compaction methods. The procedures can be automated in spreadsheet models and are intended to be used for the rapid evaluation of large inventories of canals to identify those canals that present the greatest risk for producing a failure with a large peak outflow and limited opportunity for warning, evacuation, and canal operator response that might prevent or limit the severity of a failure.

The primary factors affecting the peak breach outflow rate and the time to reach the peak outflow are the soil erodibility and the failure initiation condition and the associated hydraulic stresses applied to the soil. These together will determine whether a breach initiates and enlarges slowly or rapidly. The greatest risks are associated with highly erodible embankments experiencing overtopping flow or piping under significant head. Erosion of these embankments will progress through the breach initiation phase quickly and produce a rapid breach enlargement that causes a large peak outflow with a short time available for warning and evacuation of the nearby population or operational response to shut down and drain the canal. Highly erodible embankments experiencing low-head piping can also be a serious threat, but may experience a slower breach initiation due to the low stresses associated with piping under a low hydraulic gradient. If breach initiation can be detected at an early stage, there may be time for intervention to shut down the canal, prevent the breach, or carry out effective warning and evacuation actions.

There is a need for additional research in this area to test and prove the procedures developed herein, and to develop more detailed models for the accurate simulation of potential failures of canals of greatest concern.

Introduction and Purpose

The Bureau of Reclamation has constructed more than 8,000 miles of irrigation water delivery canals since 1902. Although typically reliable, canal failures have occurred on occasion throughout Reclamation's history. Threats to these canals include animal burrows, tree roots, embankment and foundation issues, penetrations by turnout pipes and utilities, seismic events, internal erosion under static loading, hydrologic events, and operational incidents. Canal failures can have significant consequences, and potential consequences are increasing as urban development surrounds formerly rural canals.

To understand the risks associated with individual canals, modeling of potential failures is needed. Breaching of traditional embankment dams has been widely studied and tools for predicting dam breach outflow rates are well developed and continuing to improve. However, breaching of canal embankments has not been studied extensively, and there are potentially significant differences between the canal situation and the embankment dam scenario. These include the flow of water past the developing breach, the two-dimensional nature of flow entering the breach, limitations on the ability of canals to convey water to a breach site, and wide variability in the erodibility of canal embankment materials. These factors may significantly affect the mechanics of the erosion process and the resulting breach outflow hydrograph.

To gain a better understanding of canal breach processes and develop guidance and tools for evaluating flooding risks associated with potential canal breaches, Reclamation has carried out the series of laboratory physical model tests described in this report. Small-scale models were constructed and tested to failure under controlled conditions in the indoor hydraulics laboratory in Denver, Colorado during the winter of 2010-2011. The long-term objectives of the testing were to develop straightforward relationships for predicting canal breach outflow rates as a function of canal and embankment geometry and geotechnical and erodibility characteristics and to support the development of canal-specific breach simulation models. Such tools will support rapid, appraisal-level evaluation of large numbers of canals and the detailed analysis of specific cases.

Background and Literature Review

Modeling the hydraulic consequences of dam failure is one of the classical problems of hydraulic engineering. Early hydraulic engineers considered cases of instantaneous failure of dams and attempted to predict the dynamics of resulting flood waves in downstream channels, with incremental refinements to include the effect of channel resistance and highly unsteady flows (Chow 1959). During the 1970s, interest in the topic became more urgent and practically focused following several notable dam failures and the adoption of federal dam safety rules and

legislation in the United States (Powers 2005). While early attempts at dam failure modeling had assumed instantaneous and complete dam failure, more recent practice has sought to model the dam failure process and adjust flooding predictions to account for the fact that most dams, especially embankment dams, fail gradually and partially. Wahl (1998) summarized embankment dam breach modeling methods and equations for predicting breach parameters, including breach size and shape and rate of development. These breach parameters provided as input to a dam break flood simulation model allow one to predict the outflow from a breached dam impounding a large reservoir. The most recent developments in this field have been increased two-dimensional modeling of the breach outflow flood and its inundation effects, and the development of models that simulate the detailed erosion and breach development processes of embankments (Wahl 2010). Two such models are the SIMBA/WinDAM model developed at the Agricultural Research Service (Temple et al. 2006), and HR-BREACH, developed at HR Wallingford (Mohamed 2002). Among other refinements, these models recognize distinct phases in the breach process during which different erosion mechanisms and factors are predominant. The most important distinction is between the breach initiation phase and the breach development phase. Breach initiation is characterized by relatively low flows and a slow increase in flow rate, and the embankment still retains the complete volume of the upstream reservoir. Breach development (or *breach enlargement*) is characterized by much larger flow rates and rapid increases in flow rate as well as permanent loss of storage volume in the reservoir. During breach initiation, it may be feasible to intervene and halt the breaching process, but during breach development it is no longer practical to stop the breach from enlarging.

Canals and Levees

Although much attention has been directed toward embankment dams with large reservoirs, the failure of flood levees and canal embankments is also an area of concern. Following flooding in the upper Mississippi and Missouri River basins in 1993 and in New Orleans in 2005 following hurricane Katrina, this topic has taken on greater prominence. While the Bureau of Reclamation is associated with few true levees, the 8,000+ miles of canals on Reclamation projects have become a concern as a result of increasing urbanization and some notable recent failures (Fig. 1). They share some similarities with flood levees, being very lengthy structures often constructed with available local materials and less rigorous engineering design and construction oversight than traditional embankment dams impounding large reservoirs. Reclamation is presently working to assess the risks associated with canals on our projects.

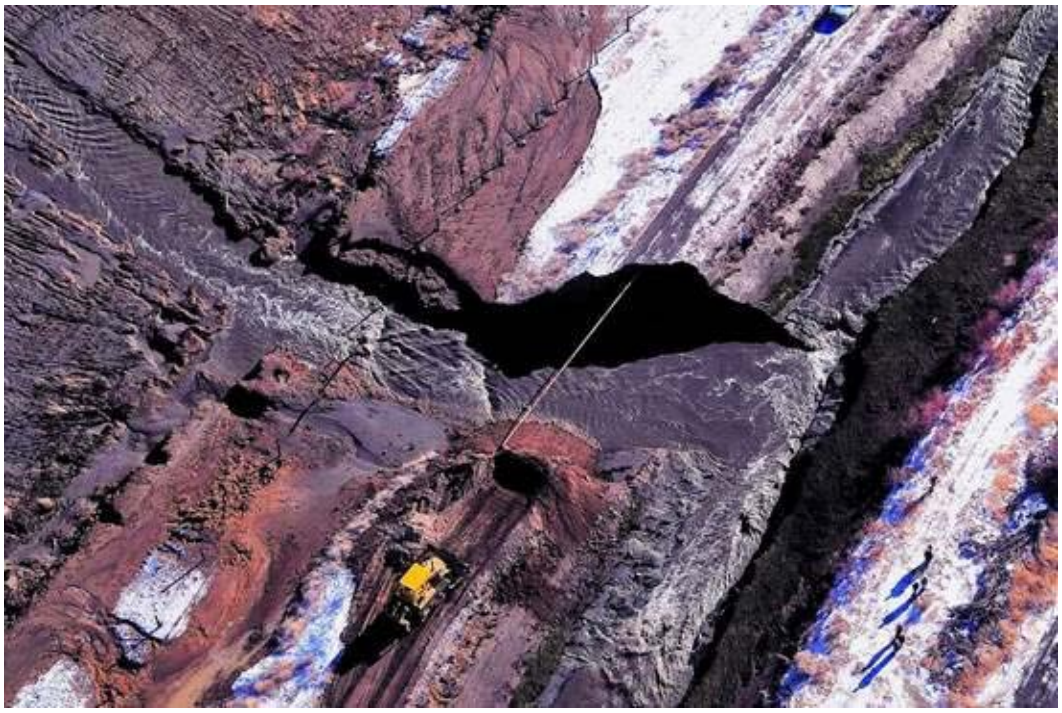

Figure 1. — Overview of the breach of the Truckee Canal near Fernley, Nevada, January 5, 2008.

Modeling Embankment Erosion Processes

The focal point for this work is the need to simulate erosion and breach processes, breach outflow hydrographs, and resulting flooding in the vicinity of potential canal breach sites. These simulations can be carried out with one or two-dimensional numerical models of the canal system and the area surrounding a potential breach site. Most existing models that might be used focus the analysis on the flow downstream from the breach, but do not directly simulate the erosion and breach processes themselves. A breach description (size, shape, rate of development) must be provided as input to such models, which calculate the breach outflow analytically, assuming that erosion takes place as prescribed. With very few previous studies considering canals specifically, breach parameters might be selected using existing guidance for traditional embankment dams, or engineering judgment (making breach size comparable to the size of the canal cross section). Wahl (1998) summarized breach parameter prediction methods available at that time and Wahl (2004) evaluated the uncertainty of predictions made using those methods. New breach parameter prediction methods have appeared in the literature recently (e.g., Xu and Zhang 2009; Pierce et al. 2010), but these have only marginally advanced the state of the art.

Physically-based erosion and dam breach models that incorporate quantitative measures of material erodibility are now under development for application to traditional embankment dams. These tools offer the potential to significantly

improve the accuracy of dam breach flood predictions when carefully applied to specific cases (Wahl 2009). Two promising models are the SIMBA/WinDAM family of models developed by the USDA-Agricultural Research Service (Temple et al. 2005, 2006; Hanson et al. 2011) and the HR-BREACH model developed at HR Wallingford in the United Kingdom (Mohamed 2002). These models have been initially developed to simulate overtopping erosion and breach of homogeneous embankments and are now being further developed to include piping erosion and zoned embankments. Both models simulate conditions on the upstream side of the embankment using level-pool reservoir routing schemes that would not be adequate to simulate the dynamics of a canal-breach situation.

Comparing Dams, Levees, and Canals

Earthen embankments may be used to create dams, levees, and canals. All are water-retaining structures, but they have different operational requirements and constraints and are significantly different when one considers the processes and consequences associated with their potential failure. Table 1 summarizes some similarities and differences between these structures.

Table 1. — Characteristics of dams, levees and canals relevant to breach modeling.

	Loading frequency	Potential for regulation during a breach event	Embankment erosion resistance	Peak outflow rate and total volume	Potential failure consequences
Dams	Constant with periodic increases in reservoir level	Limited. Flows cannot be stopped until reservoir drains.	Often moderate to high erosion resistance. Embankments usually individually engineered structures, well compacted with good construction oversight. Modern structures often contain design features that prevent internal erosion failures.	Both high. Limited only by reservoir size and breach parameters.	Extensive to catastrophic
Levees	Constant low-level loading, with episodic increases	Limited. Flows unstoppable until flood subsides or breach is plugged.	Variable. Many levees have been constructed with local materials and limited engineering and construction oversight.	Peak outflow rate usually lower due to lower head, volume large.	Localized to Extensive
Canals	Constant with varying degree of water level variation and seasonal times of non-use	High. Canal flows can be stopped and canals will drain relatively fast if check structures are available.	Variable. Many canals constructed with local materials and limited engineering and construction oversight. Many canals originally constructed in rural areas without public safety as a primary focus.	Peak outflow limited by canal capacity. Flood volume can be limited with a timely operational response.	Usually localized

Both canals and levees experience flow past the breach site as a breach develops, and this has the potential to affect the erosion and breaching process. Most laboratory experiments that have been performed to develop breach prediction models and guidance for embankment dams (Wahl 2007) have not included this flow feature. Previous laboratory work has also not considered the limiting effect of the canal conveyance capacity, since most models have provided flow to developing breaches from upstream reservoirs. Although these reservoirs have

often been limited in volume, they have generally had much greater conveyance capacity than the breach opening that was being studied.

Canal Breach Studies

Although canal breaches have occurred throughout history, there have been remarkable few efforts thus far to generalize experiences from these events. Specific canal breaches have been investigated in detail (e.g., Russell and Bountry 2008; URS 2008; McKulla 2008), but there has been little guidance for predicting the breach outflow or breach parameters for future canal breaches. Dun (2007) provided the most notable study of the hydraulics of a canal breach in a study of the Llangollen navigation canal, which failed in the United Kingdom in 2004. Dun created a numerical model for the event, simulating flow through the breach with a critical-flow section sized to match the observed breach dimensions, and limiting the breach flow with two additional critical-flow sections in the upstream and downstream reaches of the canal. The breach initiation was modeled initially as an orifice-controlled outflow, since the breach was thought to have been initiated by piping through a badger den. The model was able to reproduce the time series of observed water levels along the canal reaches. Dun did not report the modeled outflow hydrograph from the breach, although the ability to predict breach outflow hydrographs for future failures was a stated motivation for the work. Dun concluded that the hydraulics of canal breaches were significantly different from breaches of traditional dams and storage reservoirs, with the discharge from dam breaches only limited by the breach geometry, not by the upstream channel capacity. In contrast, the discharge from canal breaches can be expected to exhibit two phases, an early stage in which the discharge is limited by the breach geometry, and a later stage during which the discharge is limited by the canal capacity. Specifically, the canal capacity will be defined by critical-flow sections in the upstream and downstream reaches of the canals. These critical-flow sections will advance upstream, but their hydraulic capacity will remain essentially constant over time. In some cases, only the first phase occurs, depending on the speed of operational response by canal operators, the embankment and canal material type, the volume of water contained in the canal reach, and the geometry of the embankment (Dun 2007).

Figure 2 shows the aftermath of the breach of a large navigation canal in the United Kingdom in 1971. This canal breached into a river channel that passed beneath the canal, which was carried in an aqueduct at this location over the natural water course. As a result, the breach was able to develop to a greater depth than the canal invert elevation, making the headcuts and critical flow sections very evident in the canal reaches feeding the breach.

Figure 2. — Breach of the Bridgewater Canal, 1971. Note three people standing in the center of the breach and the large headcut that has retreated up the far reach of the canal. (Photo courtesy of Bridgewater Canal Company.)

Model Considerations

The design of a physical hydraulic model is always constrained by limitations related to laboratory space, flow capacity, model fluid and other material properties, and potential scale effects. Any attempt to model a phenomenon as complex as a canal breach will require the adoption of some simplifying assumptions. The previous work of Dun (2007) and consideration of the likely sequence of events and factors affecting the development of a canal breach led to the conclusion that it was most important for a physical model to accurately simulate local canal and embankment geometry and hydraulic conditions under the assumption of an essentially infinite canal reach and without the effects of any operational response by canal operators. The effects of an operational response and how it would interact with the hydrodynamics of the canal reach were difficult to include in a reasonably-sized physical model, so these factors were addressed separately through numerical modeling. The physical model designed according to these principles could be considered to produce a worst-case scenario brought about by any of the following conditions or combinations of conditions:

- A long reach of canal between check structures with a large volume of water to be discharged through the breach before the canal could be shut down;

- A very rapid breach due to high erodibility rates for embankment materials;

- A slow operational response due to delayed detection of a failure in progress (e.g., a failure at night in a lightly-populated area).

Such worst-case scenarios, although they may be relatively improbable, are important for risk assessment studies, as are lower-hazard scenarios that may occur with higher frequency. A worst-case scenario approach was taken for this study as a means of establishing an upper limit condition, expecting that the effects of operational responses and canal hydrodynamics could be more effectively studied analytically and numerically.

Model Scaling Laws

The key flow situation affecting this study is open channel flow in the canal and through the developing breach, and sediment detachment and transport out of the breach development zone. The key sediment detachment and transport processes are also expected to take place in zones of open-channel, free-surface flow, as headcut erosion has been shown in previous embankment breach studies to be the primary mechanism leading to embankment failure (Hanson et al. 2005). For these reasons, the model test facility designed for this study is a Froude-scaled model. The model is designed to produce equal Froude numbers in the model and prototype, with the Froude number being $\mathrm{Fr}=V/(gD)^{1/2}$, where V is the flow velocity, g is the acceleration due to gravity, and D is the hydraulic depth, equal to the cross-sectional area of the flow, A, divided by the top width of the channel, T. The Froude number is also the ratio of inertial to gravitational forces, and maintaining the ratio at a constant value in the model and prototype ensures that the gravity-driven open-channel flows are accurately reproduced in the model. Important scaling ratios for Froude-scaled models are the following:

- $Q_r = L_r^{2.5}$, where Q_r is the ratio of model and prototype discharges and L_r is the model length-scale ratio,

- $V_r = L_r^{0.5}$, where V_r is the velocity ratio, and

- $t_r = L_r^{0.5}$, where t_r is the time scale ratio.

Scaling Material Properties

The second consideration for model design is the selection of model working fluids and sediment materials. The working fluid for these models will be water, so fluid properties of model and prototype fluid are essentially the same, ignoring

minor differences caused by temperature and water quality variation. The prototype sediments in most canals are assumed to be quartz-based gravel, sand, and fine-grained soils, and similar soils were selected for use in the model. In models that simulate sediment transport, scaling of the geometric size of model sediment is important, but for this model we believe embankment erosion rates to be limited by sediment detachment processes, rather than sediment transport processes. A widely accepted model for sediment detachment is (Hanson and Cook 2004):

$$\dot{\varepsilon} = k_d\left(\tau - \tau_c\right) \tag{1}$$

where $\dot{\varepsilon}$ is the volume of material removed per unit surface area per unit time (units of velocity), τ is the applied shear stress, τ_c is the critical shear stress needed to initiate sediment detachment, and k_d is a detachment rate coefficient (units of length per time per stress). If the model scale can be kept sufficiently large that this sediment detachment model applies to both the model and prototype, then the scale ratios for these parameters can be shown to be:

- $\tau_r = L_r$
- $k_{d,r} = L_r^{-0.5}$

The critical shear stress value for most embankment materials is relatively low in comparison to the applied stresses, so τ_c is often taken to be zero in the prototype. To satisfy the scaling ratio above, the critical shear stress value for the model material should reduced from the prototype value by the length scale ratio, but if the prototype value is zero, the model value can also be set to zero.

The detachment rate coefficient scales numerically opposite to most other variables. To obtain scalable model performance, the k_d value of the model material should be larger (more rapid erosion) than the k_d value of the prototype material, and the critical shear stress should be smaller (again, more erodible). Since we are simulating generic canal embankments and not striving to model any particular embankment, we have tried to regulate k_d and τ_c to represent a range of erodibility conditions and will use the scaling relations above to relate the model values to equivalent prototype values when presenting results.

Canal Dynamics

The dynamics of canal behavior during a breach were considered in the design of the test facility. As previously stated, we strove to initially simulate a worst-case scenario in which a canal breached so rapidly, operational response was so delayed, or the canal was so long that the breach process was unaffected by the length of the reach or by operational response. In such a scenario, the water surface elevation in the canal would remain constant during the breach initiation and breach development processes and the maximum flow that could pass through

the breach would be equal to the maximum flow that could be conveyed through the two canal reaches (upstream and downstream) at that water surface elevation. This maximum flow would correspond to a critical-flow condition in each feeding canal reach, with the critical flow rate determined for the maximum available specific energy in the canal. Assuming no losses as a first approximation, this specific energy would be equal to the specific energy in the canal at the normal flow condition preceding embankment failure. Due to real hydraulic losses, such a flow condition cannot be maintained indefinitely. Further discussion of canal dynamics and the effects on peak breach outflow will be provided in the Analysis section of this report.

Model Description

Test Facility

Figure 3 shows a plan view of the physical model test facility which consists of a 70-ft long trapezoidal canal constructed between twin head boxes, one at each end of the canal. The canal was constructed with fixed, plywood walls along most of its length, with one sidewall missing in a 20-ft long centrally located embankment test section halfway between the two head boxes. Flow can be supplied into each end of the model and flow can also be released through gates located in each head box. The flow capacity into each head box is equal to the maximum theoretical critical-depth flow that can be produced in each canal reach. The gate in the west head box is oversized so that it can release the entire critical-depth flow plus the normal-depth discharge of the canal. This allows tests to be conducted with normal canal flow initially occurring past the test section. As a breach develops, the head box waste gates are throttled to keep more of the model inflow in the canal, thus providing additional flow toward the developing breach and maintaining near-normal canal water depths, simulating the slow draining of an extended-length canal reach. By accomplishing this flow change using gates, no manipulation of the output from the laboratory pumps is needed during a test.

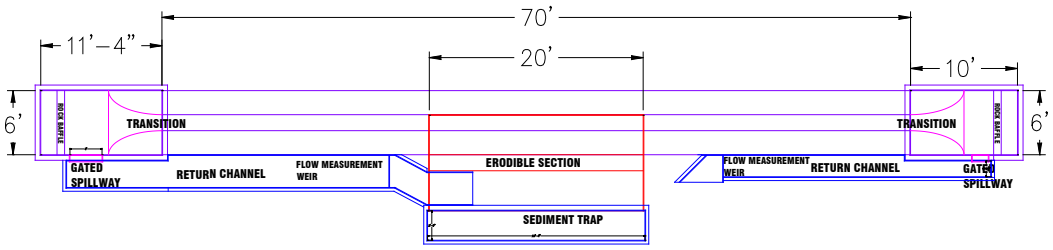

Figure 3. — Plan view of canal breach model test facility. Flow enters via the head boxes at each end of the model.

The canal cross-section used for the facility is shown in Figure 4. It was designed as a 1:16 geometric scale model of a 3,000 ft^3/s, concrete-lined trapezoidal canal, although the embankment sections were constructed without a concrete lining or any other simulated lining. The prototype canal cross section is a trapezoid with 24-ft base width, 1.5:1 (h:v) side slopes, a bed slope of 0.325 ft/mile (0.0000616 ft/ft) and a design Manning's *n* value of 0.014, yielding a normal flow depth of 16.4 ft. The model canal was constructed with no slope. Geometric scaling would have called for an elevation drop of 0.004 ft over the 70-ft length of the model, which was comparable to expected construction tolerances.

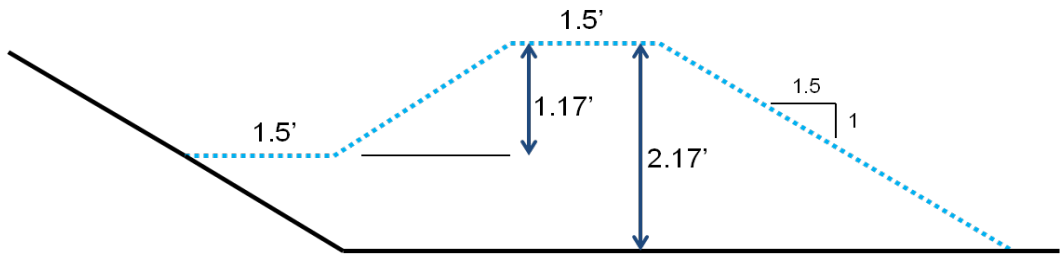

Figure 4. — Cross-section view of model canal and embankment test section.

The tested embankments were constructed in the model as simulated fill sections in a canal reach that is elevated above the surrounding landscape. On the wetted side of the embankment, the embankment crests were constructed to an elevation of 1.17 ft above the canal invert (18.67 ft prototype). On the land side of the embankment, the toe of the embankments was located 1.0 ft below the canal invert elevation. In the model, embankment material was placed in the invert of the canal to allow for potential downward erosion in this zone, and advancement of headcuts up both canal reaches away from the breach. This configuration was not a model of any specific situation in Reclamation, but was meant to be representative of many canals constructed as fill sections of varying heights. Canal reaches in deep fill sections have greater potential for embankment settling during their service lives, which could lead to a canal breach. Also, in this configuration, the breach is free to deepen below the canal invert, which will lead to the capturing of the full canal flow and the largest breach outflow.

The decision to not include a canal lining material was based on the fact that embankment breach typically takes place by headcutting, which progresses from the downstream side of the embankment toward the upstream side (toward the canal prism). Whether the driving force for erosion is an overtopping flow or piping flow through an existing flaw in the canal lining and embankment, failure takes place by erosion of embankment materials due to this flow. The lining simply collapses after the embankment has been eroded and all structural support for the lining is gone. The effect of the lining upon the critical erosion processes is minimal.

Embankment Materials

The objectives for material selection were to use embankment materials that could be placed into the model to produce erodibility characteristics representative of the range of erodibilities likely to exist in Reclamation canal embankments. No comprehensive analysis has ever been done of the erodibility of typical canal embankments either inside or outside of Reclamation, but anecdotal evidence and experience suggests that a very wide range of erodibilities is possible. Many Reclamation projects incorporate canals that were constructed as private developments without the involvement of Reclamation, so details of construction are not well known.

The physical configuration of zones within canals is a factor in their erodibility. Many canal embankments are homogeneous, but when local materials have high permeability or when a limited quantity of low permeability materials are available, the design philosophy is usually to provide seepage resistance in the form of a canal lining, either low permeability earth, concrete, or other material. However, the erodibility of the embankment as a whole will be mostly a function of the materials in the body of the embankment. Fine-grained soils, especially those with a significant clay fraction, will tend to have both low permeability and high erosion resistance, but when the amount of such materials is limited, the clayey materials will be used in the lining and the more coarse-grained (and erodible) materials will be used in the remainder of the body of the embankment. This arrangement means that the more erosion resistant lining is supported on top of a potentially erodible embankment body. During either an overtopping or piping erosion event, the main portion of the embankment will erode first via headcutting that progresses upstream toward the lining. When the lining is left unsupported, it will fail quickly as a structural element, regardless of any inherent erosion resistance it might have. This situation is analogous to the configuration of fuse plug embankments which are designed to breach quickly for the control of emergency spillways (Pugh 1985).

Recent experience from canal failures on Reclamation projects also confirms the potential for highly erodible canal embankments. Cone penetration test data from the Truckee Canal failure show that much of the embankment displays characteristics of clayey silt, sandy silt, silty sand, or sand. Samples of materials taken from this breach site were tested for erodibility by Reclamation (Erdogan and Wahl 2008) and materials from the embankment itself displayed moderate to rapid erosion rates. In-place dry unit weights of materials in the vicinity of the breach were in the range of 70 to 82% of standard Proctor maximum values.

To address the possibility of both homogeneous embankments constructed from erosion-resistant fine-grained soils and embankments constructed from more erodible materials with a low-permeability lining, a wide range of erodibility characteristics is needed. Hanson and Hunt (2007) reported the erodibility changes caused by varying compaction water content and compaction energy for two fine-grained soils typical of soils used for embankment dam construction, a

silty sand (SM) and a lean clay (CL). Erodibility of soil samples was measured using a submerged jet test (Hanson and Cook 2004). Samples were compacted from about 5% dry to 9% wet of the standard Proctor optimum water content, with compaction energy varying from standard Proctor to as low as 20% of standard Proctor. Variations of the erodibility rate coefficient were observed to be as large as two to three orders of magnitude for the lean clay and over one order of magnitude for the non-plastic SM soil.

Soil Selection and Testing

The soil selected for the canal breach tests was a silty sand (SM) with a small percentage of fine gravel and some plasticity (PI=5), purchased from a local landscaping supplier. This soil was chosen so that there would be potential for placing the test embankments in both erosion resistant and highly erodible conditions. Material properties for the test soil are summarized in Table 2.

Table 2. — Soil characterization.

Classification[a]	Grain size[b]			Plasticity Index, PI[c]	Standard Proctor Compaction[d]	
	% gravel	% sand	% fines		$\gamma_{d,max}$, lb/ft^3	w.c.$_{opt}$
SM – silty sand	6	69	25 (10% < 0.005 mm) (8% < 0.002 mm)	5	120.9	12%

Standards used to determine soil properties:
[a] ASTM D2487, USBR 5000
[b] ASTM D2487, USBR 5330
[c] ASTM D4318, USBR 5360
[d] ASTM D698A

To further characterize the properties of the test soil, specimens produced during the compaction test were evaluated for their erodibility using a submerged jet test. Procedures for performing this test and analyzing the data to determine a jet index are described in ASTM Standard D5852 (2003). The current work used the ASTM test procedures, but analyzed the data using the method of Hanson and Cook (2004), which produces values of the critical shear stress, τ_c, and the detachment rate coefficient, k_d, as defined in Eq. 1.

Figure 5 shows the results of the compaction and submerged jet tests, focusing on the detachment rate coefficient as the key parameter describing erodibility. For the standard Proctor compaction effort, the optimum water content for compaction was about 12%, while the minimum erodibility was achieved at about 13% water content. On the wet side of optimum the erodibility increased about one half order of magnitude with a 5% increase in water content. On the dry side of optimum, erodibility increases more than 2 orders of magnitude with a water content reduction of about 6%. These results are consistent with the data reported by Hanson and Hunt (2007). The curves depict performance at standard compaction effort (12,375 ft-lb/ft^3). It should be noted that with lower compactive effort, the optimum water content for that level of compactive effort will typically increase.

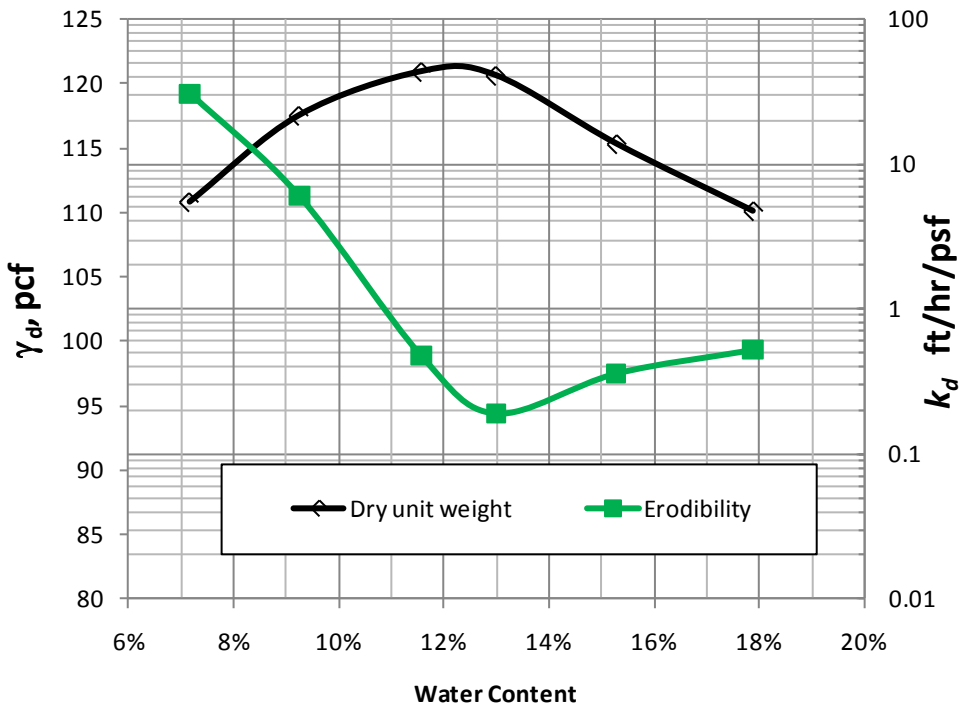

Figure 5. — Changes in dry unit weight, γ_d, and detachment rate coefficient, k_d, as a function of water content for standard Proctor compaction test specimens.

Embankment Placement and Testing

Three embankments were constructed and tested in sequence during the first phase of the research project. Soil was brought into the lab and stockpiled adjacent to the test facility where it was moistened and mixed using forklifts and front-end loaders. When the desired water content was reached, material was moved by conveyor into the test section and placed in 4- to 5-inch loose lifts, then compacted to about 3-inch lift thicknesses. All of the embankments were constructed on top of a wood-framed support table which was less firm than would be typical of compaction over a solid ground surface. This may have contributed to relatively low compacted densities, especially for the second and third embankments.

As each embankment reached the canal invert elevation, placement was temporarily halted to allow a sand cone density test and in situ submerged jet test to be run. Following the completion of these tests, the affected areas were re-filled and locally compacted, and the surface was scarified before continuing the placement operation. At the selected initial pipe elevation, a #4 (½ inch) rebar was embedded in the embankment, passing from the canal side through to the downstream side of the embankment. This rebar would later be pulled from the

embankment to start the breaching process. When embankment material had been placed to the desired finished height, each embankment and associated canal section was trimmed and finished to match a template and grid markings were then painted on the downstream face. Grid markings were painted on at 1 ft intervals horizontally, and at 0.5 ft intervals of elevation.

Test Procedures

Tests were conducted by initiating flow into both head boxes at the predetermined flow rate of 8.5 ft^3/s, which was the critical flow discharge corresponding to the specific energy available in the canal at normal-depth flow conditions. The spill gates in each head box were initially set full open, and were then gradually throttled to bring the canal water surface up to normal depth and establish the normal flow rate (2.9 ft^3/s) past the embankment test section. Because of the possibility for seepage along the contacts of the embankment and the boundaries of the test section that might cause a premature breach, no attempt was made to hold these flow conditions long enough to establish a phreatic surface in the embankment. For most tests, only a few minutes was needed to establish the starting flow condition and get it stabilized. Once the flow was stable, the rebar was loosened and pulled out of the embankment to start the test.

Still photographs were taken before, during and after each test, and a continuous HD-quality video recording was made of each test from start to finish. Before and after each test, high-resolution photographs were taken for potential post-test analysis using photogrammetry software. In situ submerged jet tests were conducted following each test at suitable locations on the remnant embankment sections.

Flow rates into the canal were held steady throughout each test using the laboratory's automatic flow control system, which utilizes venturi meters and a feedback controller to regulate a valve downstream from each flow meter. The meters are calibrated periodically using a weighing tank and have an estimated flow measurement uncertainty of ±0.5%. The discharge through the spill gate of each head box was measured using custom-built ramp flumes located in the channels that returned the waste flows back to the laboratory sump. Each ramp flume was equipped with an ultrasonic level sensor whose output was sampled and recorded on a 5-second interval with a PC-based data acquisition system. Water levels in the upstream and downstream canal reaches were also measured and recorded similarly at the two ends of the 20-ft embankment test section. At the upstream ends of each canal reach (just downstream from the transitions from the head boxes into the canals), point gages were deployed to assist in maintaining steady water levels in the canals as the breach outflow increased. Gate adjustments in each test typically took place first at the downstream head box as the breach initiated, then in the upstream head box when canal levels could not be maintained by adjusting the downstream gate. This has the effect of not artificially increasing the upstream flow rate as the breach initially develops, but

then allows it to increase when there is significant canal drawdown at the breach site. No practical method of gate manipulations can exactly replicate the dynamics of a long canal reach, but this approach yields canal flows that are a reasonable facsimile of those that would occur in a prototype situation.

Embankment 1

Following initial construction of the test facility, the first embankment was placed into the test section during a one-week period in mid-December 2010. Soil was stockpiled in the indoor laboratory and tested to determine the initial water content. Moisture was then added and the soil and water were mixed using a small skid-steer loader and forklift. The target water content for this embankment was about 12% (near optimum for standard compaction effort), and actual water content achieved was about 11%. Soil was placed in compacted lift thicknesses of about 3 inches. Following the addition of each lift, the soil was compacted using two passes of a electric vibratory compaction plate (1 hp, 1125 lbf compaction force, 3500 rpm, 12.5×17 inch compaction area), followed by one pass with a custom-made compaction plate driven by an electric jackhammer. The custom-made compactor (Fig. 6) consisted of a 7×10.5 inch rectangular steel plate with bolts installed through it to produce 20 knobs on the bottom of the plate approximately 1/2-inch diameter by 3/8-inch deep. These knobs provided kneading action similar to a sheepsfoot roller that might be used in prototype compaction of fine-grained soils.

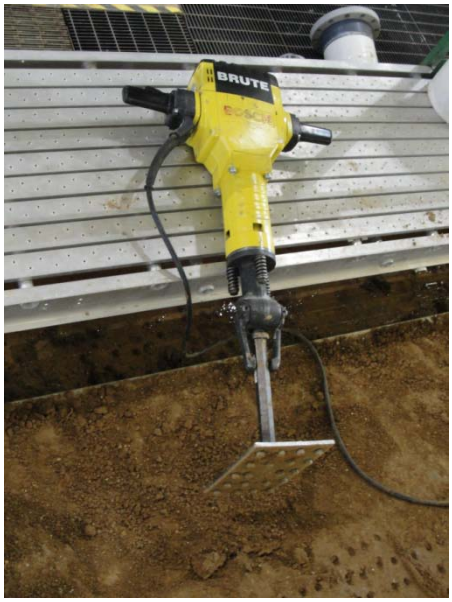

Figure 6. — Electric jackhammer fitted with custom compaction plate.

When the embankment height reached the canal invert elevation material placement was paused, and sand cone density tests and an *in situ* submerged jet test were carried out on opposite sides of the centerline of the embankment, at

approximately quarter points along the length of the test section (Figs. 7-8). The sand cone test was performed without a correction for oversize material and revealed a bulk dry density of 111.2 lb/ft^3 (92% of maximum) and water content of 11.2%. (A subsequent sand cone test on embankment 3 did apply the oversize correction, and it reduced the computed dry density by only about 1.5%). The jet test indicated a detachment rate coefficient of 0.61 ft/hr/psf. Following these tests the affected areas were overexcavated, refilled, and recompacted.

Figure 7. — Performing sand cone density test at the halfway point of embankment construction.

Figure 8. — Performing *in situ* submerged jet erosion test.

The ½-in.-diameter rebar that would be used to initiate the internal erosion failure was placed into the embankment at this point, and the embankment construction then resumed up to the desired top elevation. The embankment was then trimmed on the upstream face to match a template of the canal cross section. The

downstream face (away from the canal) was left as constructed and a painted grid system was laid out on the downstream face. Photogrammetry images were shot from overhead. The final embankment configuration prior to testing is shown in Figure 9.

The testing of embankment 1 began on the morning of December 21, 2010. The flow into the two head boxes and in the canal section was established as previously described and after a few minutes the test was initiated at about 8:10 a.m. by pulling the rebar out of the downstream side of the embankment. Formation of a small gully and headcut took place quickly and the headcut began to advance slowly upstream, into the embankment. The hydraulic gradient on the pipe at the start of the test was about 0.2 ft/ft.

After 1.8 hr (108 min) the rate of headcut advancement was very slow, so we attempted to enlarge the "pipe" by flossing the hole with a piece of nylon rope that had been laid in the embankment, parallel to the rebar that was removed to start the test. After 3.4 hr (204 min) we again enlarged the pipe using a piece of chain that was passed through the hole from upstream to downstream. At 5.83 hr (352 min) a pilot channel was cut through the crest of the embankment, approximately 6 inches wide and 3 to 4 inches deep. This pilot channel was located directly over the flowing pipe. The canal water surface was also raised artificially by about 1 inch to produce greater flow through the pilot channel. After approximately 7 hr, the pilot channel and internal erosion pipe both enlarged to the point that they joined to form a single breach opening through the embankment. At this point, the breach opening was still about 6 inches wide and as deep as the canal invert elevation, with nearly vertical sidewalls. In this condition, the model continued to operate over the course of the next two days (being shut down overnight) for a total of 21.7 hours (approx. 7-8 hours each day). Flow rate through the breach increased during this period from about 2.0 to 3.5 ft^3/s. During this time the headcut continued to advance and widen slowly. Figure 10 shows the progression of headcut advancement over the course of the test. The headcut advance rate varied from 0.006 ft/min at the start to 0.0006 ft/min near the end of the test. Figure 11 shows the change in breach width during the test, as determined from measurements taken during times when the flow was shut down. Breach widening rates varied from about 0.002 to 0.0006 ft/min, following the cutting of the pilot channel. (Note that breach widening rates throughout this report represent the sum of the erosion rates of both the left and right sides of the breach; separate erosion rates were not measured in most cases). The equivalence of the advance rate and widening rate is consistent with observations by Temple et al. (2006) in breach tests of homogeneous cohesive soil dams.

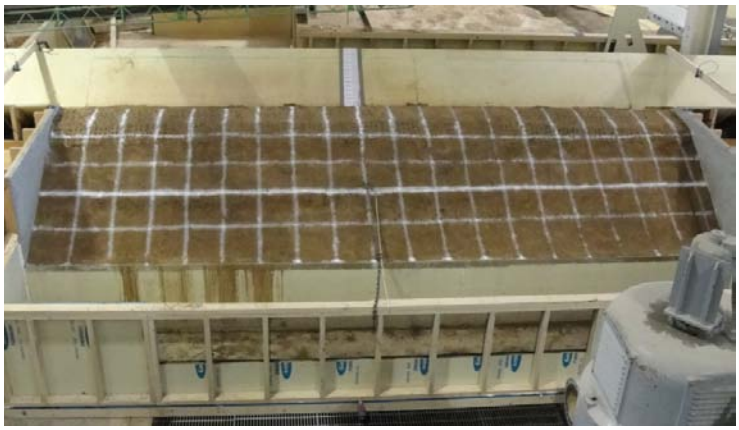

Figure 9. — Embankment 1 prior to breach testing.

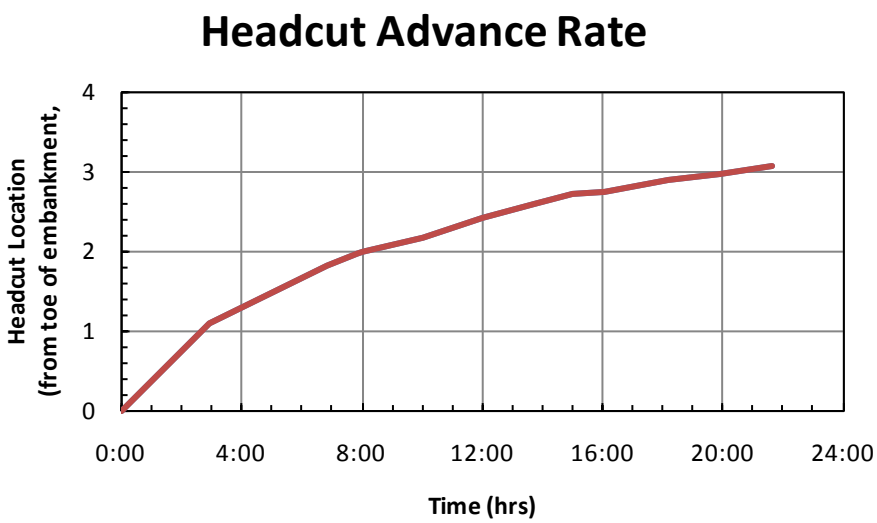

Figure 10. — Headcut migration rate into embankment 1. These data were obtained by physically probing for the headcut face and measuring its distance from a downstream reference point during the test.

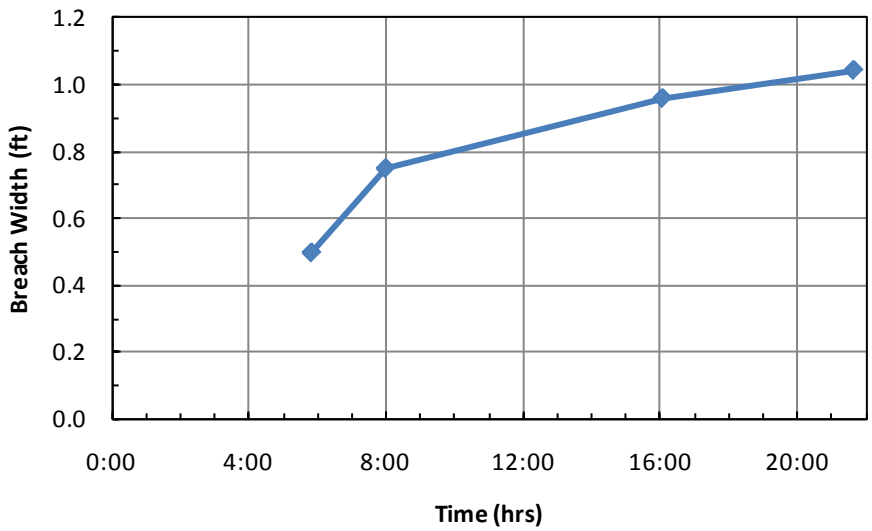

Figure 11. — Breach widening during testing of embankment 1.

Following the completion of the breach test, two additional submerged jet tests were run on benches located upstream and to either side of the breach opening (Figure 12). These tests yielded detachment rate coefficients of 0.12 and 0.06 ft/hr/psf, up to one order of magnitude more resistant than the pre-test result. This difference most likely reflects variability in the erodibility throughout the embankment. It may also be due to the fact that the pre-test value came from a location that was on the top surface of the material compacted to that point, whereas the post-test values came from surfaces that were within the body of the embankment and received additional compaction effort from layers placed above them.

Figure 12. — Post-test measurement of soil erodibility using the submerged jet test.

Figure 13 shows the canal water level and flow rate records from the test of embankment 1. Canal flow rates and water levels were steady and the breach outflow was minimal until the overtopping pilot channel was cut near the 6 hr

mark. As the breach developed, it did so slowly enough that there was essentially no spike in outflow, just a gradual increase in proportion to the enlargement of the breach. The only visible spike (at the 6 hr mark) was caused by a temporary overshot in setting canal water levels after the pilot channel was cut.

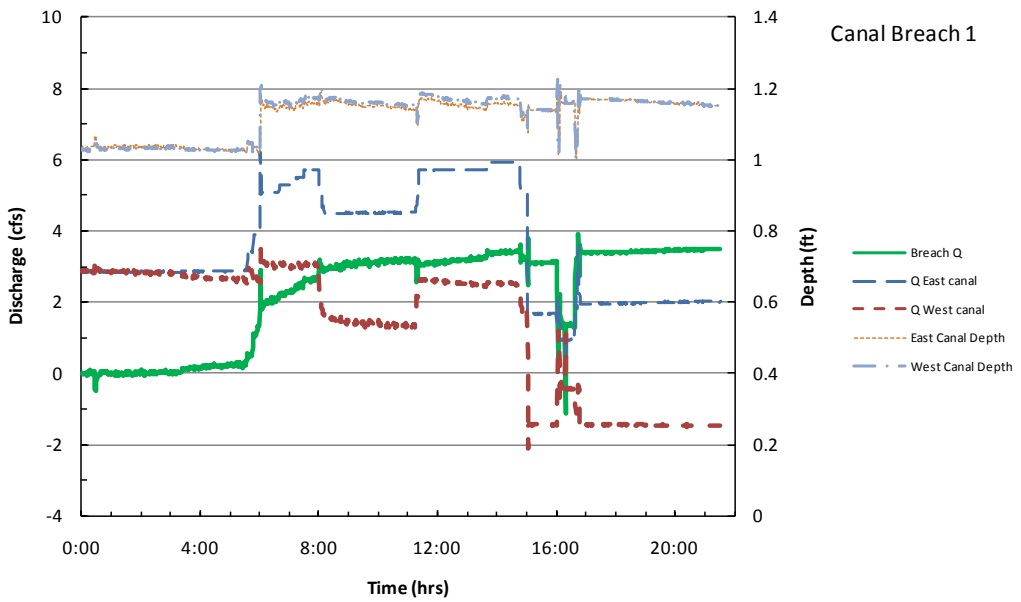

Figure 13. — Flow hydrographs and water levels from breach test of embankment 1.

Breach outflows did eventually exceed the initial normal flow rate of the canal, and there was some reverse flow and draining of the downstream (west) canal reach, but the reality of this situation is that this breach developed so slowly that canal operators would probably have the opportunity to shut down the canal once it became apparent that a failure was in progress. As a result, real breach outflows would not have exceeded the normal canal flow rate. Breach outflow exceeded the canal flow rate in this test only because we imposed a boundary condition on the test that did not reflect the likely operational response.

Embankment 2

Following the testing of embankment 1, the breached portion of the embankment was removed from the model and embankment 2 was constructed in the opening. Only about 60% of embankment 1 was removed, with remnant sections within about 4 ft of the two abutments left in place. Figure 14 shows the embankment under construction, with white lines painted on the edges of the remnants of embankment 1. The edges of embankment 1 were notched to allow embankments 1 and 2 to be keyed together. Embankment 2 was placed in a drier condition and with less compaction effort, but utilized the same rebar placement elevation for triggering the failure. Compaction consisted of four passes of the vibratory plate compactor, and the electric jackhammer was not used.

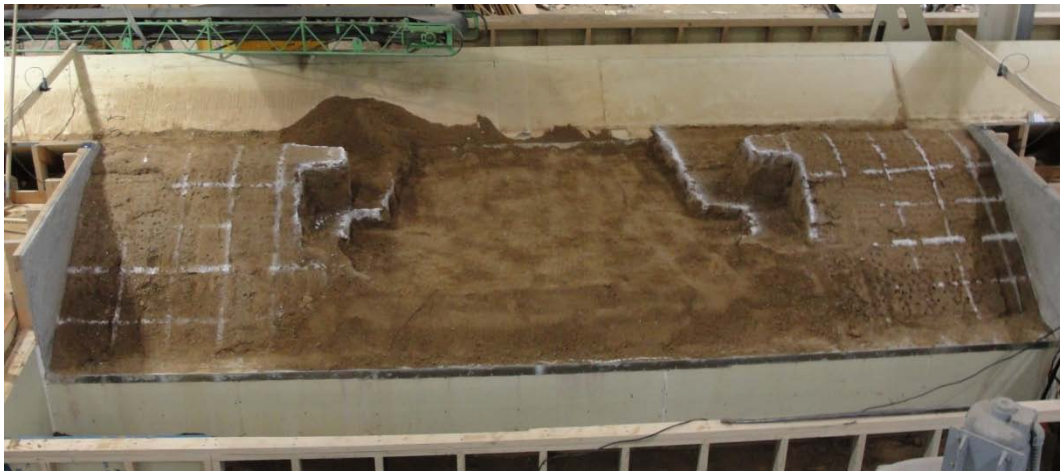

Figure 14. — Embankment 2 under construction. Remnants of embankment 1 are marked by white paint lines at the edges.

Sand cone and submerged jet tests were again performed when the embankment had been constructed up to the canal invert elevation. Bulk dry density was 92.8 lb/ft^3 (no correction for oversize material), or 77% of maximum. Water content was 8.3%, almost 4% dry of optimum for standard compaction effort, and even further dry of optimum for the reduced effort used to compact this embankment. The low density may also have been due to the fact that the embankment was constructed on a wood-framed table that vibrated somewhat during compaction. Erodibility was measured in the body of the embankment, on the downstream slope, and at two trial placement locations away from the embankment where material was compacted by the same procedures used for the embankment. Detachment rate coefficients were 20 and 43 (ft/hr)/(lb/ft^2) at the trial placement locations, 65 (ft/hr)/(lb/ft^2) in the body of the embankment, and 301 (ft/hr)/(lb/ft^2) on the downstream slope where material was probably less compacted. These values represent an increase in erodibility of about two orders of magnitude compared to embankment 1.

Embankment 2 was tested similarly to embankment 1. Erosion proceeded quickly upon removal of the rebar to start the piping failure. The headcut in the downstream slope advanced upstream and widened rapidly, and the piping hole through the embankment also enlarged simultaneously. The breach outflow began to increase rapidly about 4.5 minutes into the test. The exact time at which the headcut reached the upstream side of the embankment was difficult to discern, but at time 6 minutes there was a visible free surface in the flow through the pipe, suggesting the flow was definitely controlled at that point by the upstream end of the pipe. The dramatic flow increase beginning at 4.5 minutes suggests that the headcut beneath the pipe reached the upstream side of the embankment at about 4.5 minutes. The bridge over the enlarging pipe collapsed at 6.75 minutes, and this was approximately coincident with reaching the maximum discharge through the breach. Immediately after the bridge collapse, it was apparent that the flow rate through the breach was no longer controlled by the size of the breach opening itself, but instead two critical-flow sections had developed in the canals upstream

from each side of the breach. The breach width at this point was about 5 ft with nearly vertical sidewalls. The flow rate through the breach remained steady from this point until the flow was stopped at 8 minutes (Fig. 15). This flow rate matched the inflow boundary condition imposed upon the model. When the flow was stopped, erosion had removed essentially all of the embankment 2 material, so post-test jet erosion tests were not possible.

Because this test proceeded so rapidly, it was impossible to obtain direct measurements of the headcut position and advance rate during the test. However, video records of the test were used to reconstruct an estimate of the headcut width and breach width versus time, and this record is shown in Figure 16. The widening rate can be estimated for two distinct phases. The breach initiation phase (time 0 to 4.5 minutes) exhibits a widening rate of 0.31 ft/min, while the breach development phase (time 4.5 to 6.5 minutes) exhibits a widening rate of about 2 ft/min. The headcut advance rate can be estimated for the breach initiation phase (time 0 to 4.5 minutes) by dividing the horizontal distance from the downstream embankment toe back to the upstream embankment crest (4.76 ft) by the elapsed time of 4.5 minutes. This yields an advance rate of 1.1 ft/min which is consistent with the observed widening rates.

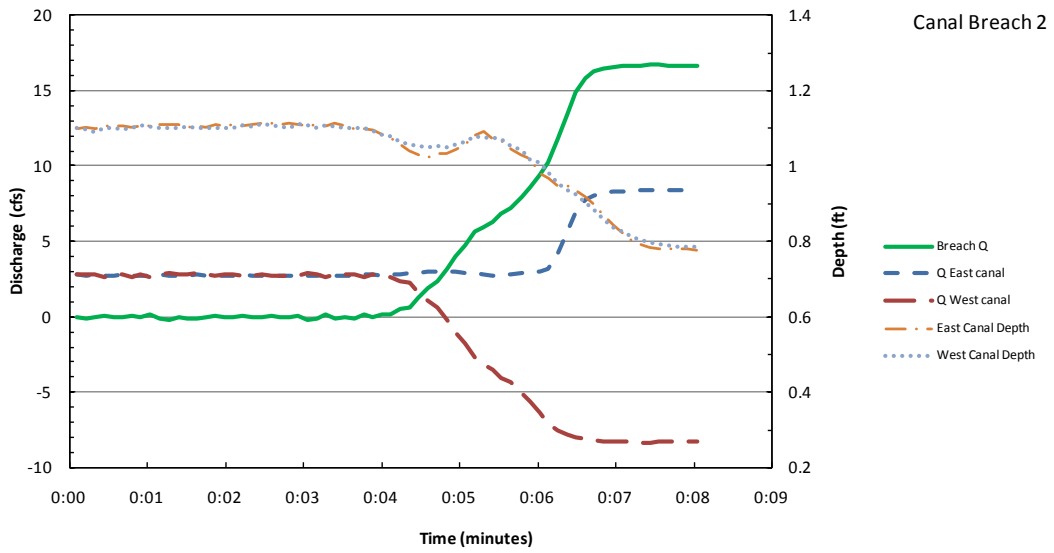

Figure 15. — Flow hydrographs and water levels from breach test of embankment 2.

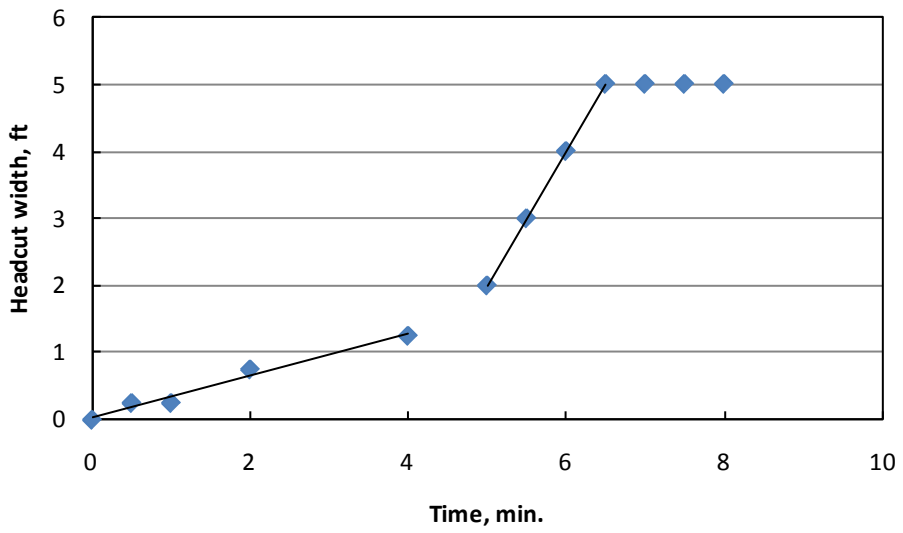

Figure 16. — Headcut and breach widths during the testing of embankment 2.

Embankment 3

Following the test of embankment 2, all soil was removed from the test section and a third embankment was constructed. Water content during soil placement was increased for this test, but compaction effort was reduced slightly to three passes of the vibratory plate. The sand cone density test on this embankment showed a bulk dry density of the compacted sand and fines of 97.7 lb/ft^3 (81% of standard Proctor maximum density), corrected for oversize material. The oversize material (>#4 sieve) was only about 4% of the sample (initial material gradation contained 6% > #4) and applying the correction reduced the determined density about 1.5%. Submerged jet tests produced detachment rate coefficients for this embankment of 32 ft/hr/psf (pre-test) and 6 ft/hr/psf (post-test).

Embankment 3 was constructed with the initial pipe defect (the #4 rebar) located about 2 inches below the normal operating water surface in the model canal. This location might simulate internal erosion through an animal burrow, since those are usually located higher in the embankment, often near the typical operating water level of the canal.

The breach initiation phase of this test proceeded slowly, despite the high erodibility of the embankment. This was due to the very low flow rate produced through the piping hole with only about 1.5 inches of head driving the flow. The estimated hydraulic gradient on the hole was 0.054 ft/ft. Although the flow rate out of the pipe was not directly measured, it did not appear to increase significantly during the time that headcut advancement was taking place, so we believe the hydraulic gradient and associated shear stress were too low in this test to cause enlargement of the hole. Flow through the hole and down the face of the

embankment did quickly create a gully and headcut on the downstream side of the embankment, and the headcut proceeded to widen and advance slowly upstream. Initially, multiple stair-stepped headcuts were visible, but the lower headcuts advanced somewhat more quickly and gradually incorporated the higher headcuts (Fig. 17). Unlike the first two tests, this embankment experienced saturation of the entire embankment over the course of the test. Within minutes of starting the test, dampness began appearing on the downstream face of the embankment, first around the edges of the embankment and gradually spreading to cover the entire surface.

Figure 18 shows that changes in headcut width were very slow during the first 3.5 hours of the test as the gully seemed to deepen down to the base of the embankment, but did not widen significantly, at least not in a visible way at the top face of the embankment. From time 3:30 to 4:45 the headcut did widen significantly and continued to advance upstream, although the flow rate still had not increased significantly. At time 4:45 the thin bridge over the pipe collapsed and the headcut began to enter the upstream side of the embankment. The headcut advance rate up to this point averaged about 0.02 ft/min. The first major collapse of the upstream side of the embankment occurred at time 4:48. The breach developed rapidly from that point on and by about 4:52 it had widened sufficiently that the flow control appeared to have shifted from the breach opening to the canals. Widening continued until time 4:56, and the breach widening rate during this phase was 0.64 ft/min. Headcut advancement up the west canal leg (the original downstream canal reach) was tracked for another 6 minutes using a probe to locate and mark the headcut face at specific times (Fig. 19), and the rate of advancement was about 0.77 ft/min.

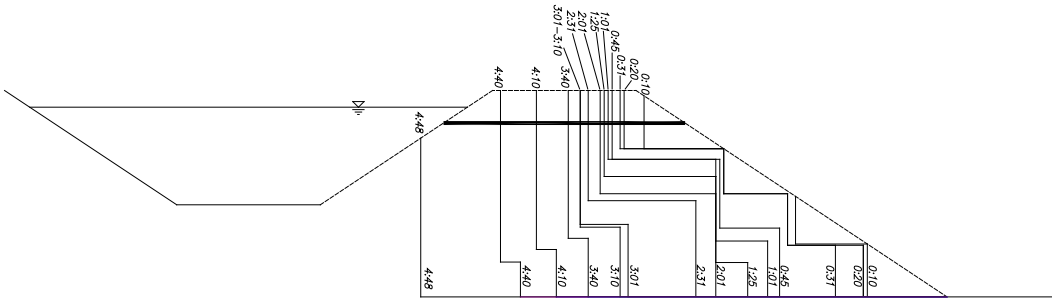

Figure 17. — Headcut advance through embankment 3 during the breach initiation phase. Labels are elapsed time in hours and minutes. Horizontal position of headcuts was determined by physically probing from downstream side of embankment. Headcut heights are estimated.

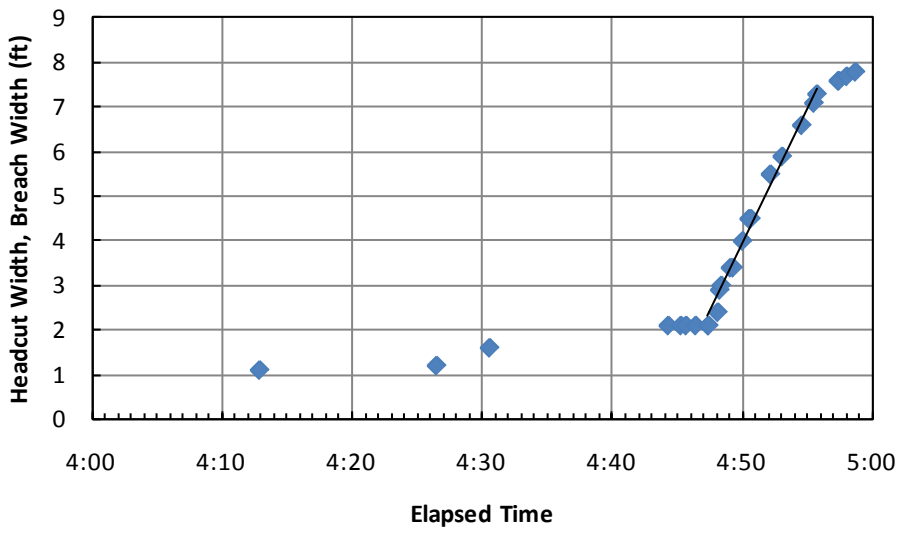

Figure 18. — Headcut and breach widening rate during breach of embankment 3. Breach widening rate during breach development phase (approximately 4:48 to 4:56) was 0.64 ft/min.

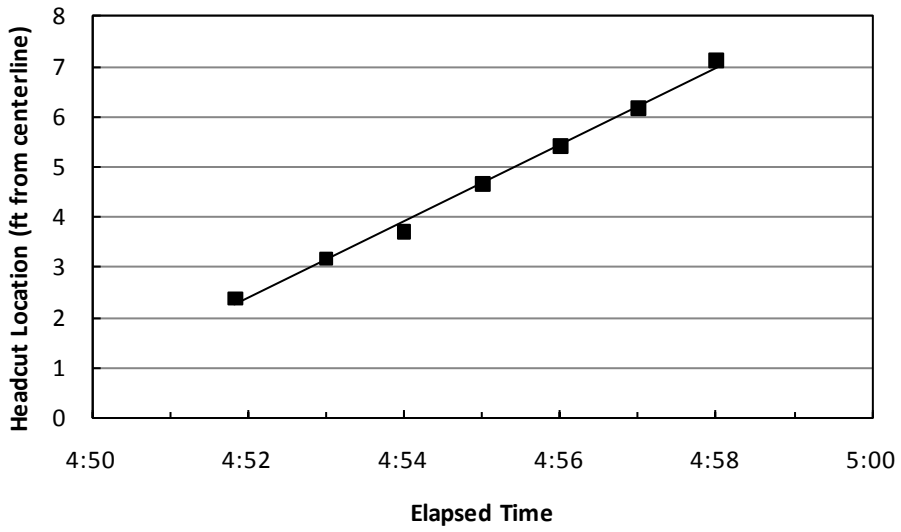

Figure 19. — Location of headcut advancing up the invert of the west (downstream) canal following breach of canal embankment. Distances are from the centerline of the breach opening. Headcut advance rate was 0.77 ft/min.

Figure 20 shows the water levels and flow hydrographs for the canals and breach opening during the test of embankment 3. The maximum breach outflow was nearly reached at about time 4:51, while breach widening was still taking place. Peak breach outflow again reached the 17 ft^3/s boundary condition imposed on the model, which is a critical-flow condition in each feeding canal having a specific energy equal to that of the canals at normal flow conditions.

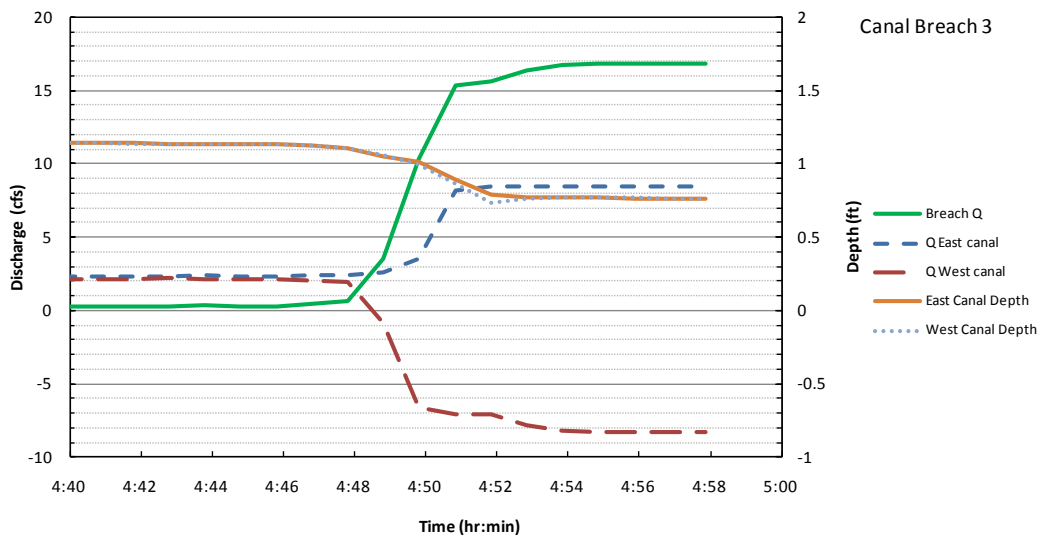

Figure 20. — Water levels and flow rates during test of embankment 3.

Discussion

Due to variation of material properties, differences in failure initiation conditions, and the highly non-linear nature of key components of the breach process, the three embankment tests effectively demonstrated a wide range of breach development behaviors, as summarized in Table 3. In this section we will examine the differences between the tests, their internal consistency to one another, and how they compare to research performed by others.

Table 3. — Breach initiation and development times from model embankment tests. Prototype values in parentheses are representative times for a prototype that is 16 times larger than the tested model.

Test	Breach initiation time Model (Prototype)	Breach development time Model (Prototype)
1	Impossible to evaluate due to interventions during test	286 hr (48 days) * Projected time to reach full breach width (5 ft), based on observed widening rate near end of test
2	4.5 min (18 min)	2.5 min (10 min)
3	4.75 hr (19 hr)	4 min (16 min)

Figure 21 shows that detachment rate coefficients, k_d, varied over about 3 orders of magnitude across the three embankments. Looking at the multiple jet tests performed on individual embankments, there is variation of about ±½ order of magnitude due to non-homogeneity and/or uncertainties in the jet test itself. Still, the measured erodibility parameters were relatively consistent with the results obtained from the compaction test specimens, considering that the densities of

embankments 2 and 3 were significantly below the standard Proctor compaction curve.

Figure 22 shows both the detachment rate coefficients and critical shear stress parameters from the pre- and post-breach jet erosion tests, relative to erodibility classes suggested by Hanson and Simon (2001). The figure also shows adjusted values representative of a hypothetical prototype structure assuming a 1:16 model-to-prototype scale ratio and the parameter scaling relations discussed earlier. The figure demonstrates that although at model scale all three of these embankments had erodibility parameters that would be characterized as moderately to very erodible, in Froude-scaled hydraulics models they are representative of prototype embankments ranging from very erodible to the edge of the very resistant category.

Overall, the erodibility of the test embankments is believed to be representative of the range of erodibilities possible in real canal embankments, including those that are poorly compacted or constructed from inherently weaker materials such as non-plastic ML and SM soils. Hanson and Hunt (2007) showed that erodibility is strongly impacted by compaction effort, compaction moisture, and soil type, and very low and very high erodibility rates can result from many different combinations of those factors.

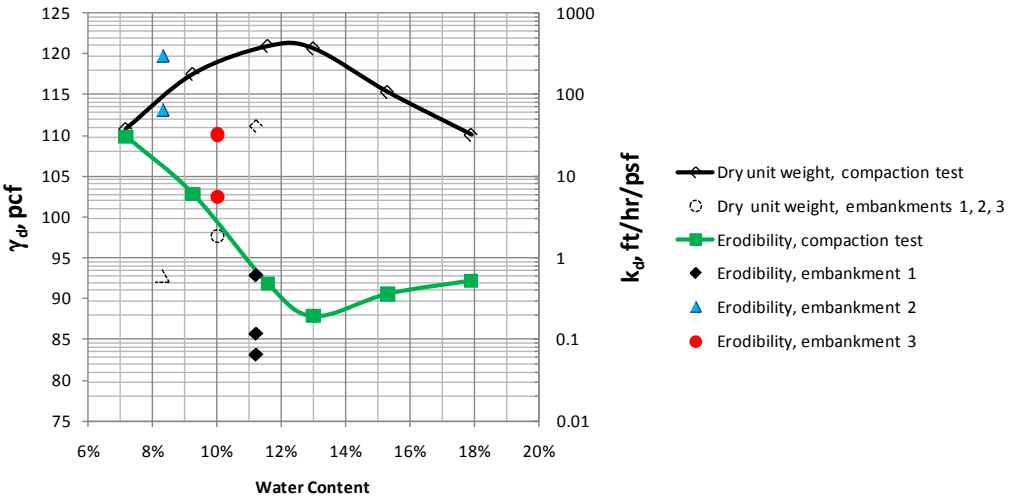

Figure 21. — Soil compaction and erodibility properties of test embankments compared to standard Proctor compaction test results.

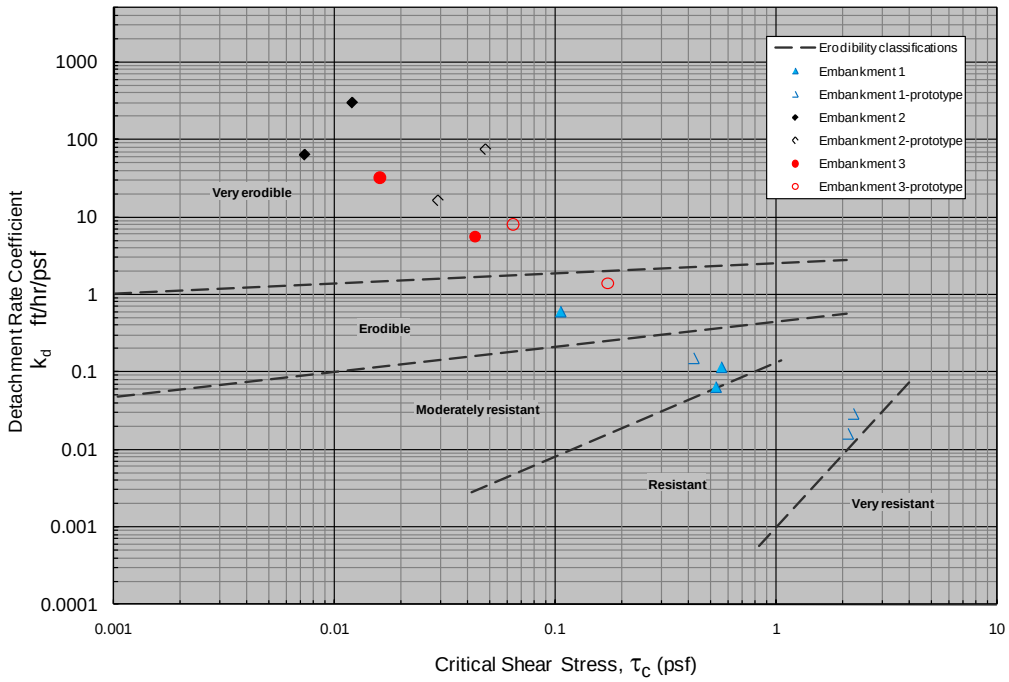

Figure 22. — Erodibility parameters of tested model canal embankments (filled symbols) and values adjusted to represent a hypothetical prototype 16 times larger than the tested model (open symbols). Erodibility classification boundaries are those proposed by Hanson and Simon (2001).

Erosion Rates

Table 4 summarizes significant results from the three canal breach tests related to erosion rates. Headcut advance and breach widening rates shown for test 1 are the range of values observed in the period after the overtopping pilot channel was opened, while erosion rates were gradually declining. For test 2, the advance rate is the nearly constant value observed for the breach initiation phase, and the widening rates are the values during breach initiation and breach development, respectively. For test 3 the headcut advance rate applies to the breach initiation phase and the widening rate is for the breach development phase, after headcut advance into the canal section was substantially complete.

Table 4. — Erosion rates during embankment breach tests.

Test	k_d (range) ft/hr/psf	Headcut advance rate ft/min	Breach widening rate ft/min
1	0.06 – 0.61	0.0006 – 0.006	0.0006 – 0.002
2	65 – 300	1.1	0.31 – 2.0
3	6 – 32	0.02	0.64

For comparison, Hunt et al. (2005) conducted breach widening tests of homogeneous silty sand and lean clay embankment dams with upstream reservoirs that were 4 ft tall with 6 ft crest widths and 3H:1V upstream and downstream slopes. The tests evaluated only the widening rate from a starting condition of a 1-ft wide notch cut entirely through the embankments from upstream to downstream toe. From these tests, an equation to predict the widening rate, *dW/dt*, was developed:

$$\frac{dW}{dt} = 2k_d \tau_{ew} = 2k_d \left[0.7\gamma_w g \left(y_c^{1/3} n / 1.49 \right)^2 \right] \tag{2}$$

where τ_{ew} is the effective stress on the breach sidewalls, γ_w is the unit weight of water, y_c is the critical flow depth approximated as two thirds of the upstream flow depth, n is the Manning's n value, taken to be 0.020, and 1.49 is a conversion factor needed to apply the equation in English units. This equation states that the erosion rate of each breach sidewall is proportional to k_d and the applied stress, implying that the critical stress to initiate erosion is nearly zero. This is the case for our canal embankments 2 and 3, where τ_c values from submerged jet tests varied from 0.007 to 0.04 lb/ft^2. For embankment 1 the τ_c value ranged from 0.1 to 0.5 lb/ft^2.

To apply this equation to the canal breach tests, we may assume y_c to be two thirds of the upstream normal flow depth in the canals, or 0.68 ft. Effective stress on the breach sidewalls is thus about 0.2 lb/ft^2 (9 Pa), or about half the stress level of the tests by Hunt et al. (2005). The breach widening rates computed from Eq. 2 are then 0.0004-0.004 ft/min for test 1, 0.13-0.39 ft/min for test 2, and 0.04-0.21 ft/min for test 3. If we drop the assumption of τ_c=0 and instead compute $dW/dt=2k_d(\tau_{ew}-\tau_c)$, then we obtain the results shown in Table 5.

Table 5. — Comparison of observed breach widening rates and those predicted using relation by Hunt et al. (2005).

Test	k_d (range) *ft/hr/psf*	τ_c *lb/ft^2*	Computed breach widening rate (Hunt et al. 2005) *ft/min*	Observed widening rate during breach development *ft/min*
1	0.06 – 0.61	0.1	0.0002 – 0.002	0.0006 – 0.002
2	65 – 300	0.01	0.4 – 1.9	2.0
3	6 – 32	0.025	0.03 – 0.18	0.64

These compare reasonably to the observed widening rates during the breach development phase of each canal breach test. Observed rates are somewhat higher, which is expected since in these tests the headcut base was deeper than the canal invert (i.e., there was a bed drop through the breach opening), whereas in the tests by Hunt et al. (2006) the breach bottom elevation was equal to the elevation of the upstream reservoir bottom and the exit channel (i.e., no bed drop through the breach opening).

Although the reasonable comparison between the observed breach widening rates and the results of Hunt et al. (2005) is reassuring, it does not appear that breach widening is a critical process affecting the determination of peak canal breach outflow, since flows quickly become canal-controlled when the breach width increases to the point at which critical-flow sections become established in the canal reaches leading to the breach. The widening rate is important in determining how quickly the peak outflow is reached, but does not have a strong influence on the magnitude of the peak outflow (unless widening takes place so slowly that flow control never shifts to the canal sections).

Breach Initiation Process

As discussed previously, there are two distinct phases of the breaching process, *breach initiation* followed by *breach development*. Breach initiation is characterized by low flows through a defect in the embankment. This defect can be an internally eroding "pipe", or overtopping flow through a locally low section of the embankment, simulated in physical models with a pilot channel. Erosion takes place relatively slowly in this phase. The key process is usually headcutting, characterized by gully development on the downstream face. In a piping failure headcutting takes place initially downstream from where the pipe exits onto the downstream face of the embankment, and eventually advances into the embankment, undercutting the exit end of the pipe. In addition to headcutting, there is the possibility for downward erosion of the pilot channel if stresses are high enough, or enlargement of the pipe along its length, again if stresses are high enough. Downward erosion of the crest of a pilot channel, enlargement of a piping hole, or shortening of a piping hole by headcutting can all increase the flow rate, accelerating the breach initiation process. Ultimately, depending on the rates of the various processes, breaching can take place either by enlargement of the original defect to the point of catastrophic failure, or by headcut advancement through the embankment driven by the flow through the defect.

The three embankment tests demonstrated two cases of relatively slow breach initiation and one case of relatively fast breach initiation. The breach initiation rate for embankment 1 was limited by the erosion resistance of the embankment, and the breach initiation rate for embankment 3 was limited by low stress applied in the piping hole flowing under a small head. Embankment 2 exhibited a high breach initiation rate due to the combination of low erosion resistance and stress levels that were high enough to cause enlargement of the pipe at the same time that headcutting was also shortening the pipe and destabilizing the embankment. It is not evident whether pipe enlargement, headcut advancement, or an accelerated combination of the two was ultimately responsible for causing the breach.

We can relate the observed breach initiation behaviors to material properties in more quantitative ways by applying numerical models of the key processes of piping erosion and headcut advancement.

Piping Erosion

For piping erosion, a numerical model of piping erosion was developed by Bonelli et al. (2006) and further developed by Bonelli and Brivois (2007) and by Wahl et al. (2008). The model predicts the increase in flow rate through a developing pipe defect as follows:

$$\frac{Q(t)}{Q_0} = \left[1 + \left(1 - \frac{\tau_c}{\tau_0}\right)\left(e^{t/t_{er}} - 1\right)\right]^{5/2} \tag{3}$$

where $Q(t)$ is the discharge at a specific time t, Q_0 is the initial discharge at time zero, τ_0 is the shear stress applied to the interior of the cylindrical hole at time zero, and t_{er} is an erosion time scale parameter determined from

$$t_{er} = \frac{2L_{\text{pipe}}}{k_d \gamma_w H_{\text{pipe}}} \tag{4}$$

where L_{pipe} is the length of the hole, γ_w is the unit weight of water, and H_{pipe} is the head differential across the hole. It is important to note that the k_d parameter in Eq. 4 is assumed to be obtained from a hole erosion test (HET), an alternative test for measuring erodibility parameters of fine-grained soils. Wahl et al. (2008) showed that the k_d values obtained from submerged jet erosion testing tend to be higher than the values obtained from the HET, typically by about one order of magnitude. Similarly, critical shear stress values obtained from jet testing tend to be lower than HET results, often by about two orders of magnitude.

Values of the initial discharge, Q_0, and initial shear stress applied in the hole, τ_0, were computed for each test. Initial discharge estimates were made by applying the energy equation and assuming a Darcy friction factor f=0.050. Shear stress was estimated by applying the momentum equation to the hole, computing $\tau_0=\gamma_w S d_{\text{pipe}}/4$, where γ_w is the unit weight of water, S is the hydraulic gradient, and d_{pipe} is the initial hole diameter, taken to be 0.5 in. for all three tests. Constructing a spreadsheet model for equations 3 and 4 and inserting the parameters for each test it was found that accurate prediction of the time scale of the breach initiation process could not be achieved without significant calibration adjustment of the critical shear stress parameter. Using the jet test τ_c values increased by two orders of magnitude led to the conclusion that applied stresses in the pre-formed erosion hole for all tests were too low to overcome the critical shear stress and enlarge the hole. The testing clearly indicated otherwise, especially for embankment 2. Using the τ_c values without adjustment and reducing the k_d values by one order of magnitude led to more useful results. The time scale of breach test 2 was predicted to be about 5 minutes, with the model predicting that flow rates through the hole would reach 1 ft^3/s at time 5 minutes and increase to 8.5 ft^3/s by time 7 minutes. This is consistent with the observed behavior. Modeling embankments 1 and 3 similarly to embankment 2, the model predicts that breach initiation for embankment 1 would have a time scale of about 24 hours (300 times as long as

embankment 2), and breach initiation of embankment 3 would have a time scale of about 70 minutes (15 times as long). In reality, embankment 1 eroded so slowly that we intervened to accelerate the breach initiation, and the breach initiation phase for embankment 3 lasted 285 minutes (63 times as long).

The numerical piping model is extremely sensitive to the values of τ_c and k_d, but does exhibit reasonable relative predictions for the three breach tests. It should be kept in mind that equations 3 and 4 simulate only the process of pipe enlargement. However, headcut advancement that simultaneously shortens the piping hole was also a factor in these tests, and could occur in other situations to which these equations might be applied. It is evident that accurate numerical modeling of the breach initiation process is a very challenging problem due to the variability of materials, uncertainties in our ability to determine erodibility parameters, and interactions between simultaneously occurring erosion processes. To apply such a model to a hypothetical real event, an additional challenge would be specifying the starting point for the analysis. Some initial pipe size and associated flow rate need to be assumed, as the model is not capable of simulating the process starting from a time of absolutely zero flow; a finite flow rate through an existing defect is required.

Headcut Advance

A straightforward headcut model that can be applied to the headcut processes observed during breach initiation in these tests is the Temple/Hanson model (Temple et al. 2005), which relates the headcut advance rate to the rate of energy dissipation and material properties:

$$\frac{dX}{dt} = C\left(qH_h\right)^{1/3} \tag{5}$$

where dX/dt is the rate of headcut advance, q is the unit discharge in the headcut area, H_h is the vertical headcut height, and C is an advance rate coefficient. For each test, estimates were made of the unit discharge, headcut height, and advance rate, and the value of C was then computed. For embankment 1 the headcut advance period followed the cutting of the pilot channel and continued until the end of the test, since the breach opening never advanced fully through the base of the embankment and into the canal invert. Estimates of unit discharge were obtained from the breach width records depicted in Figure 11 and the breach outflow rates shown in Figure 13. The unit discharge was nearly steady throughout the headcut advance period at about 3.5 $ft^3/s/ft$. The headcut height was estimated to be 0.97 ft for the entire time of interest.

Embankment 2 experienced very rapid breach, with simultaneous enlargement of the initial pipe and headcutting back into the embankment beneath the pipe elevation. The headcut advance rate was estimated from the embankment geometry and the observation that the headcut progressed from the downstream toe to the upstream crest in about 4.5 minutes. The unit discharge was estimated by using the energy equation to compute the initial piping flow rate through the

0.5-in. diameter hole, assuming a Darcy friction factor of f=0.05 for the hole, and assigning this discharge to a 0.44-in. wide section of the embankment (converting the round hole to a square of equivalent area. The unit discharge clearly increased over the course of the test, especially near the end of the breach initiation phase, but the starting unit discharge was taken as a reference value. The headcut height was again taken to be 0.97 ft.

Embankment 3 was modeled in a similar way, with the head driving flow through the piping hole reduced to 1.5 in. and the headcut height increased to reflect the higher elevation of the initial pipe. The headcut advance rate was estimated by a single average value representing the bulk rate from the start of the test to the end of breach initiation.

Figure 23 summarizes the results graphically, with comparison to a relation proposed by Hanson et al. (2011) from flume headcut advance data originally reported in Hanson et al. (2001). The equation shown applies when k_d is specified in ft/hr/psf. If k_d is given in customary metric units of cm^3/(N-s), then the relation becomes C=0.25k_d and the units of C are still $s^{1/3}$/hr. The units conversion equation for k_d is 1 cm^3/(N-s)=0.5655 ft/hr/psf. Note that when applying equation 5, q and H_h should be given in consistent units, such as ft^3/s/ft and ft, or m^3/s/m and m; the headcut advance rate dX/dt will be computed in units of ft/hr or m/hr.

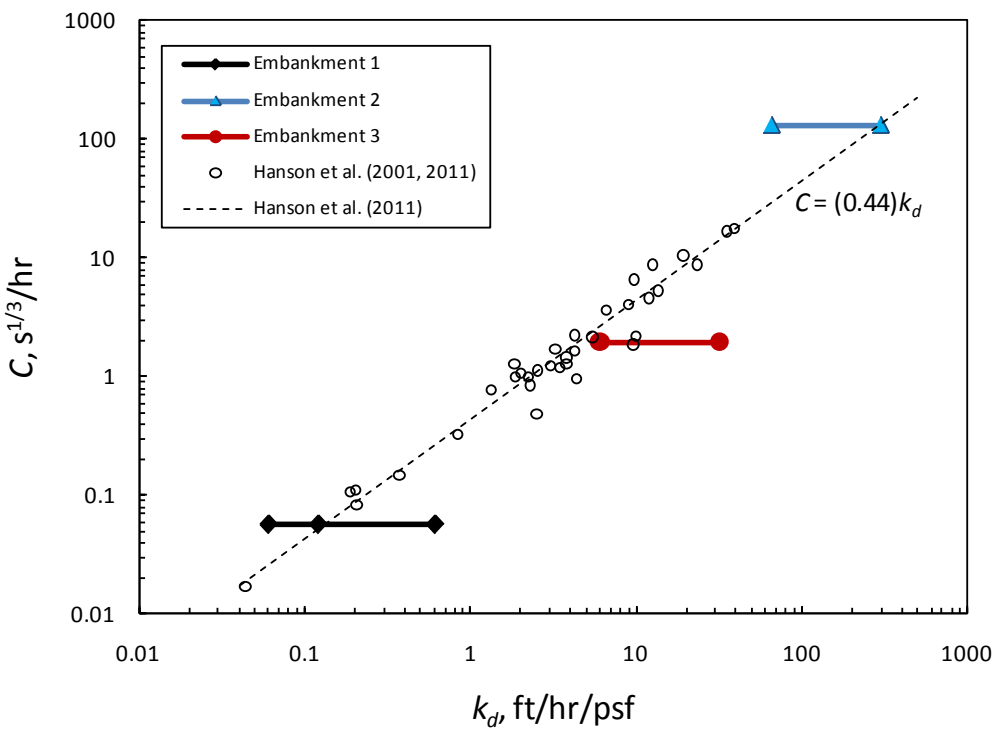

Figure 23. — Relation between headcut advance rate coefficients and soil detachment rate coefficients. Data points represent the range of pre-and post-test jet erosion test results for each embankment.

Agreement between the headcut advance rates in these tests and the relation proposed by Hanson et al. (2011) is good, considering that these tests were affected by several complicating factors compared to the original flume headcut advance experiments of Hanson et al. (2001). This is an encouraging result that suggests the WinDAM model (Temple et al. 2006; Hanson et al. 2011) can be applied to the modeling of canal embankment breach processes.

Comparison to Embankment Dam Breaches

Some additional general observations can be made from the three canal breach tests. Initial objectives of this research were to identify similarities and differences between canal embankment breaches and traditional embankment dam breaches. Potential sources of differences were the effects of flow past the breach opening, the need for the breach flow to negotiate a sharp curve to exit the canal, and the limited ability of the canal to convey flow to the breach site.

No significant differences in the rates of breach widening on opposite sides of the breach were noted. Although at times during the tests it did appear that there was some asymmetry of breach development, the asymmetry tended to balance out over the long term and final breach openings were relatively symmetric. This suggests that no adjustments or special modeling efforts need to be made to account for differences between the three-dimensional flow fields associated with a canal breach and a traditional embankment dam breach.

Flow past the breach openings as they developed also seemed to have very little impact on the breach development process. As breach size became significant, the flow conditions approaching the breach came to closely resemble flow conditions seen in the breaching of traditional embankment dams. Given the other uncertainties involved in model breach development (soil properties), it is probably not worthwhile to make canal-specific refinements to estimates of discharge coefficients for flow through canal breach openings.

Effects of Canal Hydrodynamics

The most important questions to answer regarding the potential failure of a canal embankment are the magnitude and duration of the peak outflow from the breach. This will affect the severity of flooding conditions in the vicinity of the breach and the degree to which severe flood conditions persist as distance from the breach increases. The test facility constructed for this research and the manner in which the tests were run assumed that the canal reach containing the breach was essentially infinite in length with sufficient storage in the canal prism to keep canal water levels near the normal pool level as the breach developed. Inflow to the model canals was set based on a critical-flow boundary condition for the two canal reaches upstream and downstream from the breach site that was established

with an assumption of zero energy loss in the canal. The model also assumed no effective operational response by canal operators, such as closing down nearby check gates in the upstream and downstream canal reaches to limit inflow to the breach site and the volume of water that could be released through a breach. All of these assumptions are biased toward producing the maximum theoretically possible peak breach outflow.

Due to physical limitations of the laboratory, there was no effective way to model the behavior of a finite but realistic canal reach length, short of doing sophisticated real-time numerical modeling to determine the proper inflow to each end of the test facility as the tests were in progress. The realistic boundary condition would have been a canal reach of appropriate model-scaled length with a check structure at the end of it that either admitted flow into the reach (upstream canal) or released flow out of the reach (downstream canal), with check structure flow rates defined by a gate rating relationship and with the possibility that the gates could be closed down by canal operators if it was known that a breach was in progress. The much simpler boundary condition that was used for the model was to make inflow to the test reach equal to the maximum theoretically possible critical flow rate in the canal based on its cross section size and normal operating water level.

Regardless of operational response or the length of the upstream and downstream canal reaches, even this critical flow condition is not fully realistic, as it can only be sustained for a limited period of time. To illustrate, it will be helpful to work with an example situation. The example canal has the following properties:

- Trapezoidal section, base width = 24 ft, side slopes = 1.5H:1V,
- Bed slope = 0.325 ft/mile (0.00006155 ft/ft),
- Design discharge, Q = 3,000 ft^3/s,
- Manning's n=0.014, yielding a normal flow depth y_n = 16.4 ft. The Froude number for normal-depth conditions is 0.20.

The specific energy of the canal at normal depth is = 16.63 ft. For critical flow the Froude number is $\mathrm{Fr} = V/(gD)^{1/2} = 1$, where D is the hydraulic depth A/T, A is the cross-sectional area of the channel, and T is the top width. Combining these equations we can solve iteratively to find that a critical depth of 12.33 ft has the same specific energy as the normal depth flow. The associated critical discharge is 8721 ft^3/s, which is equivalent to 8.52 ft^3/s in a 1:16 Froude-scaled model. This is the flow rate that would occur in the upstream reach of the canal if there were an instantaneous failure of the canal bank that was large enough that the breach opening did not control the flow; the flow would be controlled instead by a critical section in the canal. This ignores the energy losses and momentum changes that would be required to accelerate the flow from its normal-depth velocity to the new critical-depth velocity. For the downstream

canal, it also ignores the fact that the flow would be required to reverse its direction. If both canals delivered this flow to the breach site, the maximum peak breach outflow would be 17,442 ft^3/s.

This breach outflow rate obviously cannot be sustained indefinitely, since only 3,000 ft^3/s is entering the canal at the upstream boundary of the area of interest. To get a sense for how long this flow rate can be sustained we can compute a direct-step water surface profile in the upstream canal for the critical flow rate starting from the computed critical depth. We find that the water surface profile quickly exceeds the canal's normal depth and that the computed upstream normal depth for this flow is over 27 ft. This is due to the fact that there are real energy losses as we compute the flow profile in the upstream direction, and the flow at the critical section can only be sustained if there is a greater energy available upstream.

Since the flow rate into the upstream end of the reach remains 3,000 ft^3/s (assuming no operational response), the long-term equilibrium condition will be a flow rate of 3,000 ft^3/s along the full length of the canal, with critical depth at the downstream end of the reach (at the breach site). The flow rate of 8721 ft^3/s that occurs immediately after an instantaneous breach can only be sustained until the water surface profile is drawn down to reach the "8721 cfs critical" profile shown in Figure 24. Beyond that time, the water surface profile in the canal would continue to decline as the canal drained, gradually approaching a standard M2 profile for the 3,000 ft^3/s flow rate. Flow would be critical at the downstream end of the reach and approach normal depth at the upstream end. The downstream canal would similarly drain and undergo a transient period, but at an even faster rate since water at the downstream end of that reach would be flowing away from the breach until the effect of the breach propagated to the end of the reach. The downstream canal would eventually reach a condition of zero flow toward the breach.

The length of time required for the transition from the immediate post-breach condition to the long-term steady state will depend upon the length of the canal reach, the size of the canal cross-section, the canal slope, and many other factors. Even the beginning and ending flow conditions for the transient period are variables, since the rate of breach development will affect how closely the immediate post-breach outflow matches the theoretical upper limit, and actions taken by the canal operators may change the long-term steady state condition. None of these factors that affect the dynamic response of the canal can be adequately accounted for in a purely physical model.

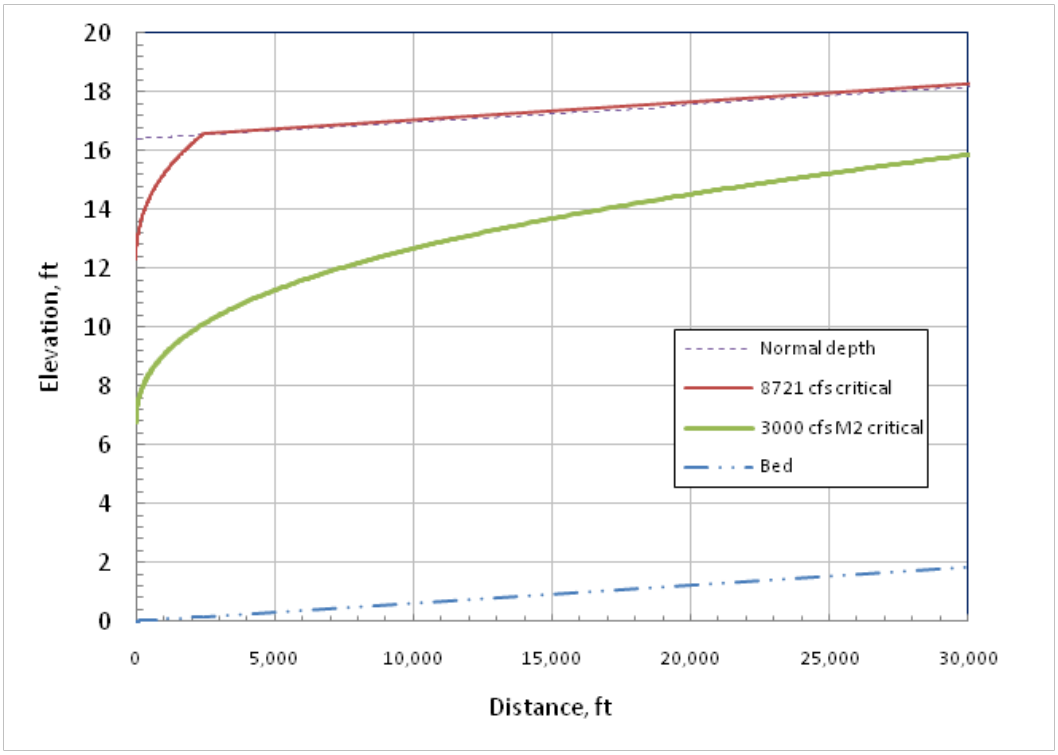

Figure 24. — Example water surface profiles computed for upstream canal following canal breach.

HEC-RAS Modeling

To illustrate the previously discussed principles further and demonstrate how canal and breach properties affect the dynamic response of a canal, a numerical model of a canal experiencing a breach failure was created using the HEC-RAS modeling suite (Hydrologic Engineering Center 2010). The model takes advantage of unsteady flow modeling and breach simulation capability to determine breach outflow hydrographs and the dynamic response of the canal reaches. HEC-RAS does not simulate actual embankment erosion processes, but does allow the simulation of different breach development rates through the selection of a total breach development time and geometric parameters describing the ultimate breach size and shape.

The basic configuration of the HEC-RAS models was a single HEC-RAS river reach varying from 2 to 100 miles in length. Within a short 400-ft reach of the canal located at the midpoint of the reach, one side of the canal was defined to be a lateral structure that would be breached at varying rates. HEC-RAS provides an option for the flow through this breached lateral structure to “leave” the model without the need for defining any other river channel reach to carry the flow away. Thus, the breach outflow is unaffected by any downstream tailwater that would be caused by the breach outflow. This was appropriate for the situation we were modeling of a fill section elevated above the surrounding landscape. The

location of the breach and the lengths of the canal upstream and downstream from the breach site were varied to produce simulations with the following length characteristics:

- 1 mile of canal upstream and downstream from the breach site,
- 2 miles of canal upstream and downstream from the breach site,
- 2 miles of canal upstream and 50 miles of canal downstream, and
- 50 miles of canal upstream and downstream.

The modeled canal used the same cross section and channel slope as the example canal used in the previous discussion section. Starting conditions for the simulations was normal-depth flow throughout the model at a flow rate of 3,000 ft^3/s. The boundary condition at the downstream end of the model was a normal-depth flow condition, with a fixed discharge of 3,000 ft^3/s. The boundary condition at the upstream end was a constant inflow of 3,000 ft^3/s, consistent with an assumption that canal operators are not able to immediately react to the breach as it is occurring (because the breach happens too quickly, there are no eyewitnesses and no remote indications of a breach, or remote indications are not immediately acted upon).

Neither boundary condition is perfectly realistic. The upstream and downstream canals would most likely terminate at gated check structures in real cases. At the downstream end, there is eventually a possibility for reverse-flow into the canal reach if the check structure is not closed down, and this reverse-flow would be controlled by an appropriate rating curve for the check structure and its gates. However, until the effects of the breach propagate down to the downstream boundary, the normal-depth outflow is a relatively accurate boundary condition. At the upstream boundary, a constant inflow is realistic until the water surface profile below the upstream check structure starts to drop. At this point, flow would increase through this check structure if it has not been closed down, and this increase would be controlled by the discharge rating curve of the check structure and its gates. Modeling either of the boundary conditions more accurately in HEC-RAS would require specification of details of the check structures and modeling of the adjacent canal pools.

The lateral structure in the model was defined to be 10 ft deeper than the elevation of the canal invert, in an attempt to create geometry similar to the physical model, where the land-side embankment toe extended to a lower elevation than the canal invert (i.e., a canal constructed in a fill section). This was only partially effective, as it was found that breaches defined to extend to much deeper elevations captured too much of the canal flow and caused cross sections of the model in the immediate vicinity of the breach to go dry, precipitating model instability. Ultimately, for stable model behavior it was determined that breach openings could extend only about 1 or 2 ft lower than the canal invert, but needed to remain high enough that a fraction of the upstream canal flow continued past the breach into the downstream canal reach. This kept the model from going dry at any cross

section. More sophisticated 2D modeling tools might handle this situation in a better way, but the HEC-RAS model was sufficient for the purposes of this study.

The breach initiation mechanism was selected to be a piping failure growing linearly from zero to 200 ft wide. The pipe was assumed to form initially at a point near the canal invert elevation, as in physical embankment tests 1 and 2, and enlarged vertically to the top of the embankment and down to the determined minimum elevation, 1 to 2 ft lower than the canal invert as described previously. The width of the breach was selected to be large enough that the breach at its full width would capture the great majority of the flow from the upstream canal and would not be the hydraulic control on the outflow. Critical-flow calculations through a rectangular breach opening suggested that control would shift from the breach opening to the canals when the breach width exceeds about 85 ft. The wider 200 ft width was selected to ensure that outflows would not be sensitive to the breach size, and this was confirmed with subsequent testing of the HEC-RAS model. However, the breach could not be made so wide and deep that it truly captured all of the upstream flow, as this would cause the model to compute "dry" cross sections, which were numerically unstable. Breach development times varying from 15 seconds up to 6 hours were used, and breaches were initiated after about 8 minutes of steady, normal-depth flow simulation. The fastest of these breach development times are clearly unrealistic for most canals, but they were selected to allow for the best possible definition of a relationship between peak breach outflow and breach development time over a wide range of conditions.

Figure 25 shows typical results of a model run, with the breach occurring halfway between check structures located 4 miles apart. The breach development time for this case is 6 min, a relatively fast breach. The three water surface profiles in Figure 25(a) show the start of the simulation, the peak outflow from the breach at t=14 min, and t=60 min, respectively. Figure 25(b) shows the outflow hydrograph (Flow Leaving), and the flow hydrographs for the upstream and downstream canal reaches. The peak breach outflow is about 11,800 ft^3/s, but reduces back to about 6,000 ft^3/s at time 30 min. Reverse flow exceeding 4,000 ft^3/s occurs in the downstream canal, and the peak flow rate in the upstream canal is about 7,300 ft^3/s. Notable features of this simulation are the transition from the very steep initial water surface profile in the upstream canal toward the 3,000 ft^3/s M2 profile after an extended period of time, and the significant draining of the downstream canal reach. This draining would be dependent on actions being taken at the downstream check structure to prevent reverse flow. The downstream boundary condition of normal depth flow is not fully realistic. A more realistic boundary condition would be a rating curve for the check structure, which would include the possibility for reverse flow if the canal water level declined rapidly enough to create a reverse head differential at the check structure.

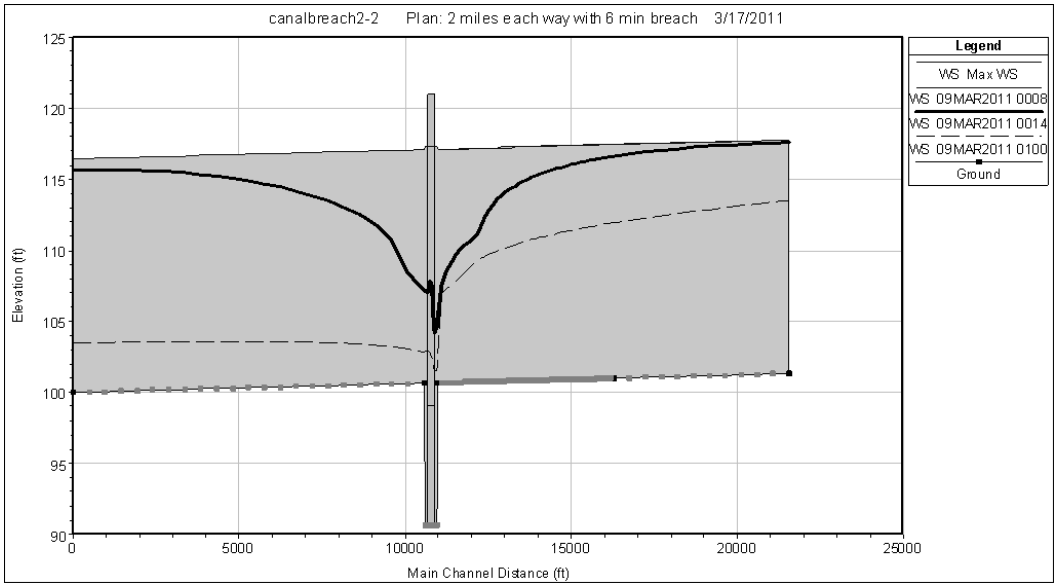

(a)

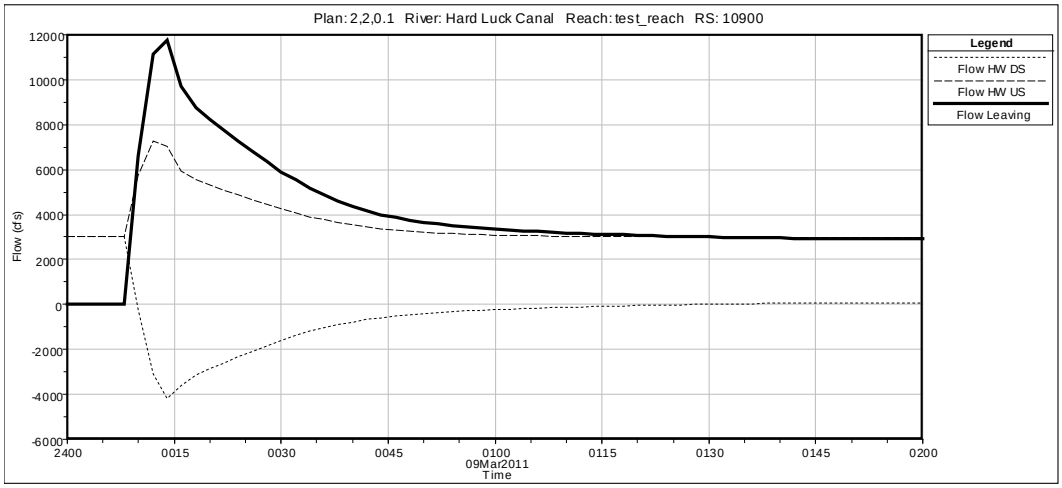

(b)

Figure 25. —HEC-RAS simulation of 6 min breach of example canal embankment with 2 miles distance to nearest upstream and downstream check structures. In (a), initial canal flow is from right to left.

Figure 26 shows the behavior with much longer 50-mile canal reaches upstream and downstream from the breach site. The breach development time is still 6 min, and the peak outflow rate is about the same, but the larger volume of water available in the longer canal reaches leads to a much slower decline of the breach outflow hydrograph. Behavior of the upstream canal is very similar in this case to the previous scenario. The downstream canal behavior is more realistically simulated in this case, since the 50 mile distance to the downstream check structure is so great that the effects of the breach on the water surface profile have not yet reached the downstream end of the model after a time of 1 hr.

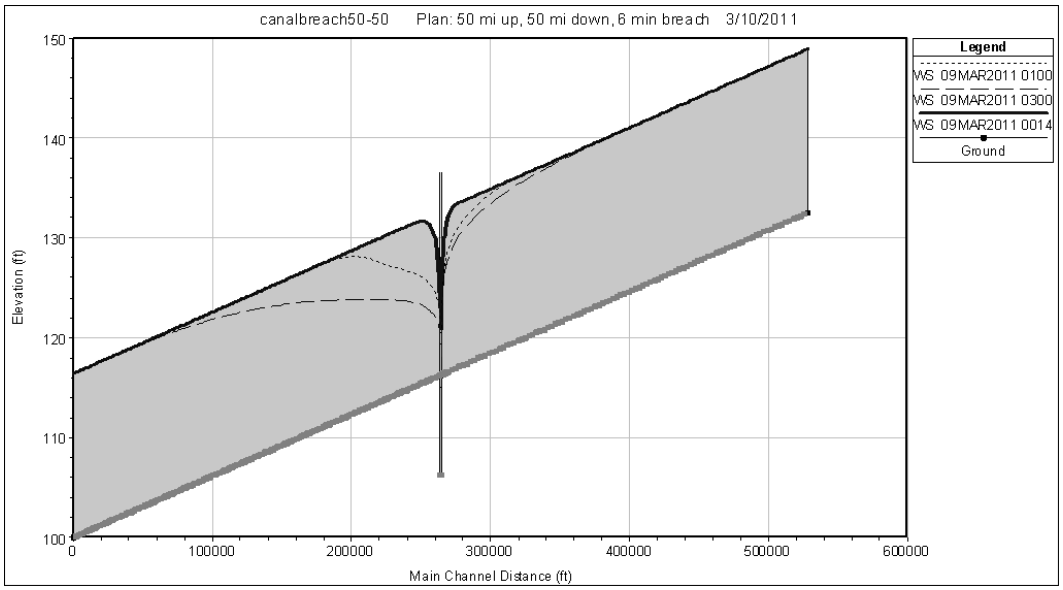

(a)

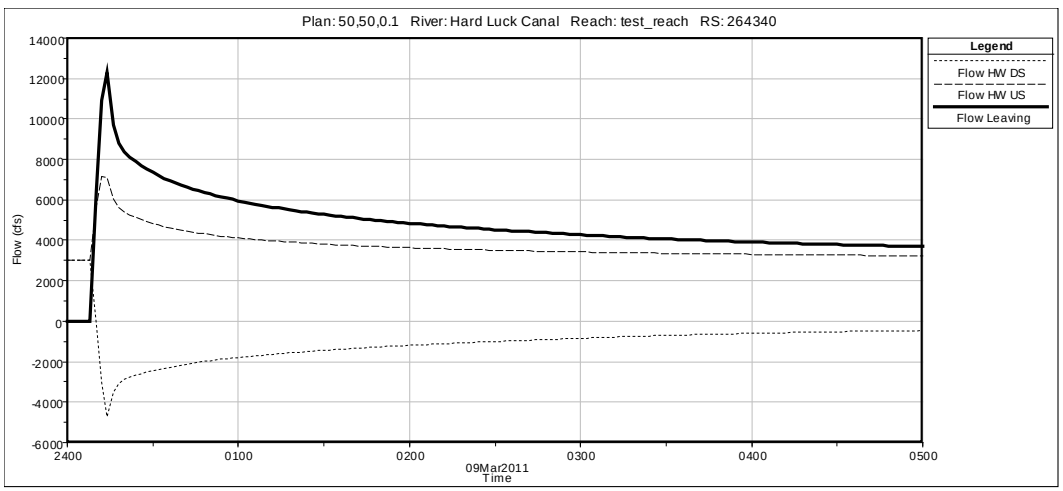

(b)

Figure 26. —HEC-RAS simulation of 6 min breach of example canal embankment with 50 miles distance to nearest upstream and downstream check structures. In (a), initial canal flow is from right to left.

Figure 27 demonstrates the effects of faster and slower breach development times with the breach located halfway between two check structures that are 4 miles apart (similar canal reach lengths as Figure 25). With a breach development time of 2 hr the peak breach outflow is reduced to about 6,700 ft^3/s occurring about 44 min after the start of the breach process (before the breach is fully formed), while a 1 min breach produces a peak outflow of 16,200 ft^3/s. This latter value is approaching the theoretical upper limit that we previously calculated to be 17,442 ft^3/s.

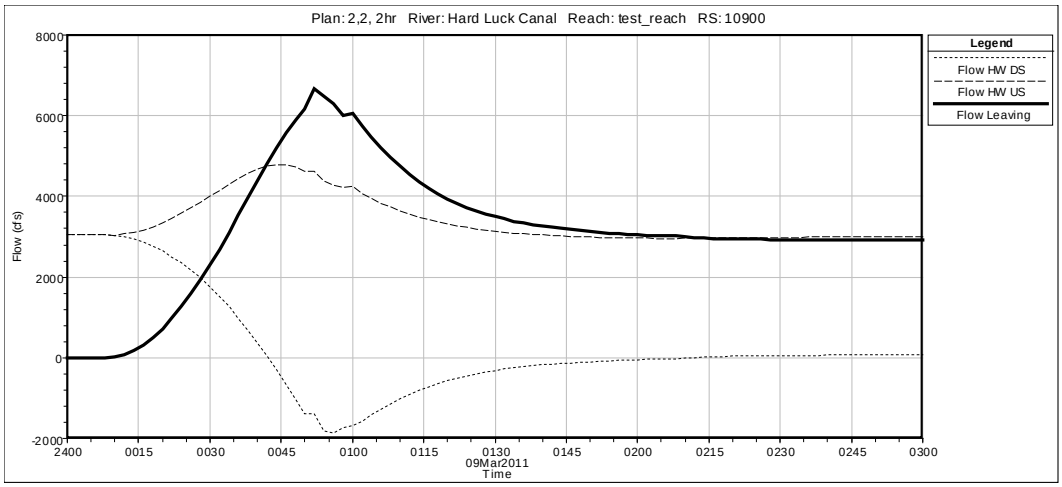

(a)

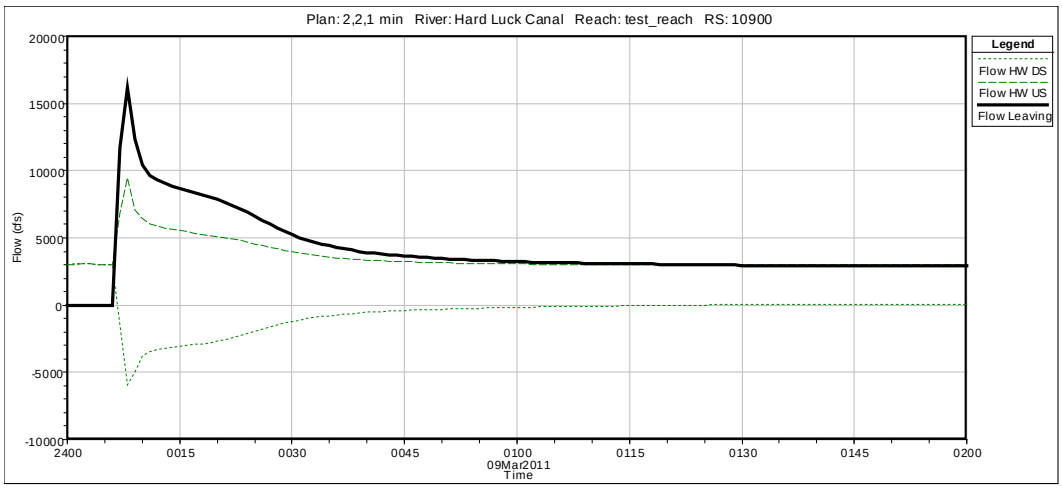

(b)

Figure 27. —Differences in simulated breach outflow for breach development times of (a) 2 hr and (b) 1 min. The breaches are located at the midpoint of a 4-mile long canal reach between two check structures with a 3,000 ft^3/s constant inflow boundary condition at the upstream end and a normal depth boundary condition at the downstream end.

Table 6 shows results of all of the HEC-RAS simulations for the example canal. The times shown from the peak outflow condition to 50% recession are the elapsed times from the peak outflow to the time at which the flow rate drops halfway back to the long-term equilibrium flow in the canal. For example, if the normal discharge in the canal was 3,000 ft^3/s and the peak breach outflow was 15,000 ft^3/s (a 12,000 ft^3/s increase), the 50% recession point would be reached when the breach outflow receded back by 6,000 ft^3/s to a flow rate of 9,000 ft^3/s. The table shows that peak outflow rates are not affected by the length of the upstream canal and are also relatively insensitive to the length of the downstream canal. Peak outflow is very sensitive to changes in the breach development time. The hydrograph recession time exhibits a more complex behavior. It is clearly sensitive to the breach development time with fast breaches exhibiting a rapid

drop in outflow after the peak breach flow occurs. Sensitivity to the upstream and downstream reach length seems to be dependent on the breach development time. Breaches that develop slowly have outflow hydrographs whose recession limb duration increases with reach length, while breaches that develop quickly recede quickly even when the reach length is large. These observations of the effect of canal reach length can also be extended to the effects of operational responses at check structures, since the closing of a check structure effectively truncates the canal reach length. The intuitive result is that the value of an operational response is greatest when a breach develops slowly and the reach length is short.

Table 6. — Characteristics of breach outflow hydrographs for HEC-RAS simulations of the breach of the example canal.

Reach Length		Breach development time	Peak outflow Q_{peak}	Time from peak to 50% recession
upstream	Downstream			
mi	*mi*	*min*	*ft³/s*	*min*
1	1	6	11,100	4
1	1	120	5,500	12
2	2	0.25	16,100	4
2	2	1	16,200	4
2	2	6	11,800	10
2	2	120	6,700	18
2	2	240	5,200	18
50	2	6	11,800	10
2	50	6	12,300	10
50	50	1	17,400	3
50	50	6	12,300	12
50	50	120	7,900	54
50	50	360	6,200	54

To facilitate the development of predictive relations for estimating breach outflow hydrograph parameters, additional HEC-RAS simulations were carried out on a smaller hypothetical canal consisting of a trapezoidal channel with 14 ft bottom width, 3:1 side slopes, design flow rate of 700 ft^3/s, channel slopes varying from 1 to 2 ft per mile, and Manning roughness coefficients of n=0.014 and n=0.024. This range of values provided scenarios with varying normal flow depths and canal Froude numbers at normal-depth conditions varying from 0.19 to 0.44. Five HEC-RAS breach simulations were carried out on the varying forms of this hypothetical canal with upstream and downstream reach lengths also varied from one-eighth mile to 2 miles. The results were consistent with those in table 6 and helped to fill data gaps, but did not materially change the dimensionless relations that were subsequently developed.

To develop relations applicable to canals of varying sizes and other properties, the following dimensionless parameters were computed for each scenario:

- Dimensionless upstream and downstream canal reach lengths, $L^*_{us}=L_{us}/R_h$ and $L^*_{ds}=L_{ds}/R_h$, where L is the canal reach length, "us" and "ds" indicate

upstream and downstream, respectively, and R_h is the hydraulic radius of the canal for normal-depth flow conditions;

- $t^*_f = t_f/t_{ref}$, where t_f is the breach development time and t_{ref} is a reference time scale computed as the hydraulic depth of the canal at normal depth conditions, $D=A/T$, divided by the wave celerity, $(gD)^{0.5}$. This simplifies to $t_{ref} = (D/g)^{0.5}$;
- $Q^*_{peak} = Q_{peak}/Q_{c,max}$, where Q_{peak} is the maximum breach outflow and $Q_{c,max}$ is the sum of the maximum theoretical discharges through the upstream and downstream canal sections when critical flow occurs with a specific energy equal to the specific energy in the canal at normal-depth flow conditions; and
- $t^*_{recession} = t_{recession}/t_f$, where $t_{recession}$ is the recession time defined previously and shown in Table 6.

It should be noted that when calculating the dimensionless times, values of the breach development time, t_f, were adjusted from the values shown in Table 6 to the time that would have been required for the breach width to reach just the point at which hydraulic control shifts from the breach opening to the supplying canals.

Figure 28 shows the relation between dimensionless peak discharge and the dimensionless breach development time. The proposed upper envelope curve indicates the highest peak outflow likely to be obtained for a given breach development time. Data points lying closest to the upper envelope curve are generally those for the cases with very long canal reaches downstream and upstream from the breach site. Data points lying well below the envelope curve are associated with shorter canal reaches.

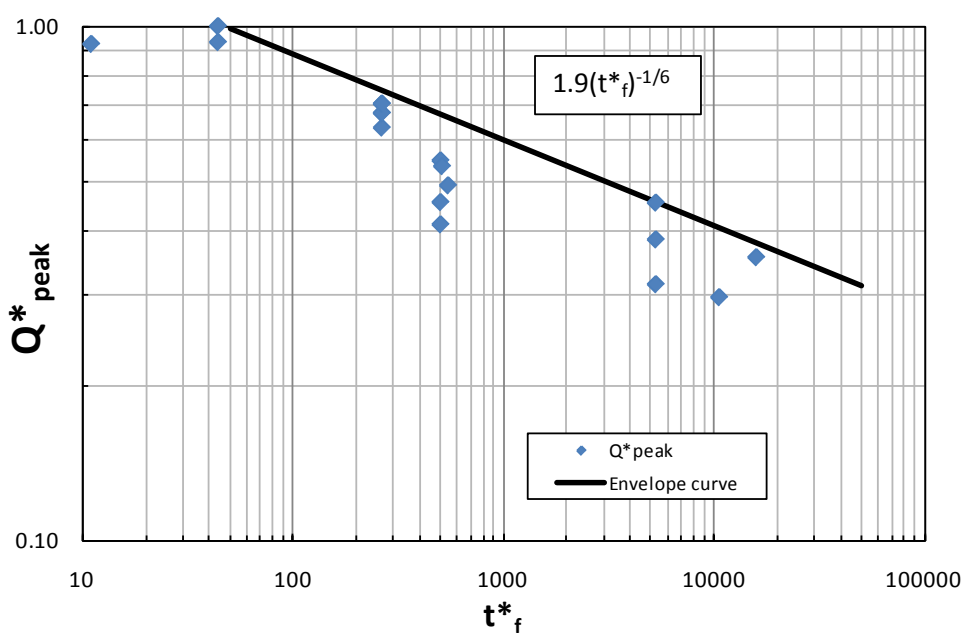

Figure 28. — Dimensionless peak discharge as a function of dimensionless breach development time.

The most important factor affecting the proximity to the envelope curve seems to be the downstream canal reach length, as Table 6 previously showed that the peak outflow is more sensitive to the downstream reach length than the upstream reach length. This is likely due to the fact that until the upstream canal is shut down, it provides water to the breach site at a rate that is not dependent on the reach length (critical flow prevails). In contrast, the downstream canal immediately begins to drain and although critical flow also prevails from that direction, the energy available to drive the critical flow condition diminishes as the downstream reach drains. To quantify the effect of the downstream reach, for each case the ratio $Q^*_{peak}/Q^*_{envelope}$ was computed, where $Q^*_{envelope}=1.9(t^*_f)^{-1/6}$. Figure 29 shows how this ratio varies as a function of the dimensionless downstream-canal reach length. Again, an upper envelope curve is shown that will allow one to make conservative estimates of the percentage of the peak flow that could be developed in a canal with a specific downstream reach length. The curve envelops most of the simulations carried out for this study and has the desirable properties of tending toward 1.0 for long canal reaches and toward zero when the canal reach length is very short. Clearly there is some scatter in the data, indicating that other factors have some influence, but the canal reach length appears to be a useful predictive parameter. Combining these two relations, the predictive equation for dimensionless peak discharge is

$$Q^*_{\text{peak}} = \frac{1.9}{(t^*_{\text{f}})^{1/6}}\left[1-\frac{1}{(L^*_{\text{ds}})^{1/3}}\right] \tag{6}$$

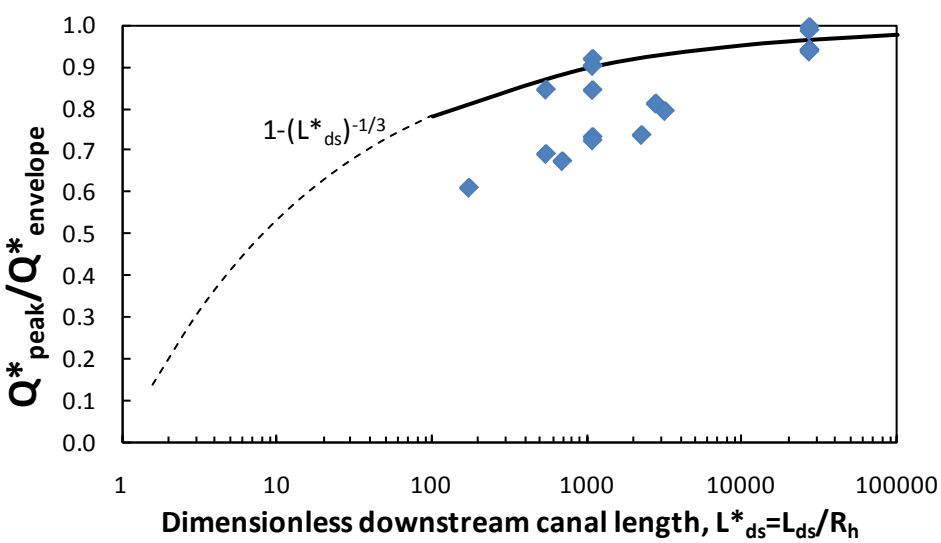

Figure 29. — Effect of downstream canal reach length on peak breach outflow.

The final aspect of a canal breach outflow hydrograph that is of significant interest is the duration of high flows following the peak outflow. Assuming no operational response that shortens the duration, the most useful predictive relation that could be determined from these simulations is shown in Figure 30. The

dimensionless time required for the flow to recede 50% of the way back to the normal canal flow rate is inversely related to the dimensionless breach development time. Again, the figure shows that other factors also affect the recession time, but the relation to the breach development time should be useful for predictive purposes. Note that although the figure shows the dimensionless recession time increasing for rapid failures (small values of t^*_f), since the time reference for the recession time is the breach time itself, the net result is that rapid failures still experience more rapid recessions than do slow failures, which is consistent with the HEC-RAS results shown in Table 6.

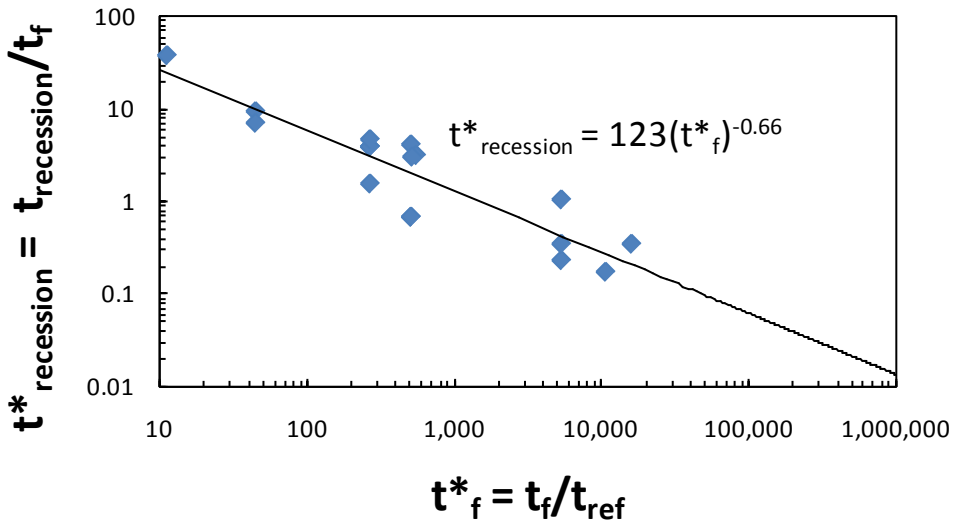

Figure 30. — Hydrograph recession time as a function of breach development time.

Appraisal-Level Estimates of Canal Breach Hydrographs

The essential characteristics of a canal breach hydrograph are the time required for breach initiation, the time required for breach development, and the resulting breach outflow hydrograph. The hydrograph may be defined by the peak outflow magnitude, the time at which peak outflow occurs, and the time required for the hydrograph to recede. The physical embankment breach tests and HEC-RAS modeling described in this report provide a basis for estimating all of these characteristics of a canal breach event.

Breach Initiation

Breach initiation may take place through one or a combination of three different processes, headcut advance caused by overtopping flow, headcut advance due to

flow through a piping defect that is not enlarging significantly, or direct erosional enlargement of a piping defect. The latter process is the most difficult to model analytically, so estimates of breach initiation time due to piping should be based on the headcut advance failure mechanism. However, models for all three processes will be outlined here.

Breach Initiation by Headcut Advance due to Overtopping Flow

Consider the canal embankment shown in Figure 31. Flow overtops the embankment with head H_{ov}. The unit discharge over the embankment can be estimated from a broad-crested weir equation as $q=2.6H_{ov}^{1.5}$ with H_{ov} in ft and q in $ft^3/s/ft$. For metric units of m and $m^3/s/m$ the coefficient 2.6 $ft^{1/2}/s$ becomes 1.44 $m^{1/2}/s$. Assuming that headcutting initiates at the toe of the embankment, the time for breach initiation is the time required for the headcut to advance a distance L back to the upstream edge of the embankment crest. The headcut advance rate can be estimated from Eq. 5 as $C(qH_h)^{1/3}$, with $C=0.44k_d$, with k_d obtained from a submerged jet erosion test and given in units of ft/hr/psf. If k_d is given in metric units of $cm^3/(N\text{-}s)$, then $C=0.25k_d$. If a jet test is unavailable, values of k_d and τ_c may be estimated using Table 7 and Table 8 (Hanson et al. 2010) which relate k_d and τ_c to the clay content, compaction effort, and water content during compaction.

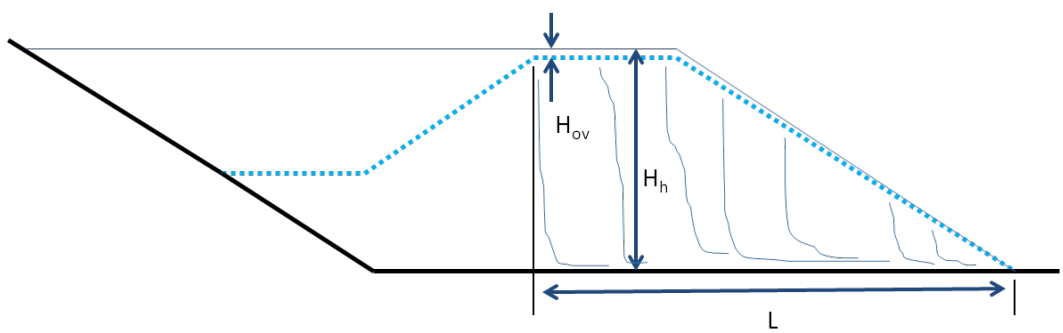

Figure 31. — Canal embankment parameters for estimating headcut advance rate due to overtopping flow.

Combining these equations together, the time for breach initiation in hours is:

$$t_{\text{initiation}} = \frac{L}{(0.44k_d)(2.6H_{ov}^{1.5}H_h)^{1/3}} \tag{7}$$

with L, H_h, and H_{ov} given in ft and k_d in ft/hr/psf.

Table 7. — Approximate values of k_d in $cm^3/(N\text{-}s)$ as a function of compaction conditions and % clay (Hanson et al. 2010). [1 $cm^3/(N\text{-}s)$ = 0.5655 ft/hr/psf]

% Clay (<0.002 mm)	Modified Compaction (56,250 ft-lb/ft^3)		Standard Compaction (12,375 ft-lb/ft^3)		Low Compaction (2,475 ft-lb/ft^3)	
	≥Opt WC%	<Opt WC%	≥Opt WC%	<Opt WC%	≥Opt WC%	<Opt WC%
	Erodibility, k_d, $cm^3/(N{\cdot}s)$					
>25	0.05	0.5	0.1	1	0.2	2
14-25	0.5	5	1	10	2	20
8-13	5	50	10	100	20	200
0-7	50	200	100	400	200	800

Table 8. — Approximate values of τ_c in Pa as a function of compaction conditions and % clay (Hanson et al. 2010). [1 Pa = 0.0209 psf]

% Clay (<0.002 mm)	Modified Compaction (56,250 ft-lb/ft^3)		Standard Compaction (12,375 ft-lb/ft^3)		Low Compaction (2,475 ft-lb/ft^3)	
	≥Opt WC%	<Opt WC%	≥Opt WC%	<Opt WC%	≥Opt WC%	<Opt WC%
	Critical shear stress, τ_c, Pa					
>25	16	0.16	4	0	1	0
14-25	0.16	0	0	0	0	0
8-13	0	0	0	0	0	0
0-7	0	0	0	0	0	0

Breach Initiation by Headcut Advance due to Piping Flow

Analysis of this case is similar to the previous situation, except that the overtopping flow is replaced by orifice flow through a piping defect in the embankment. The elevation of this defect and its diameter and length must be specified to allow estimation of the flow rate through the pipe. The starting diameter should be a practical value relating to the size of piping defect that might prompt notice of the piping condition by project personnel and begin the cycle of potential operational responses to a canal emergency. The key variables are illustrated in Figure 32.

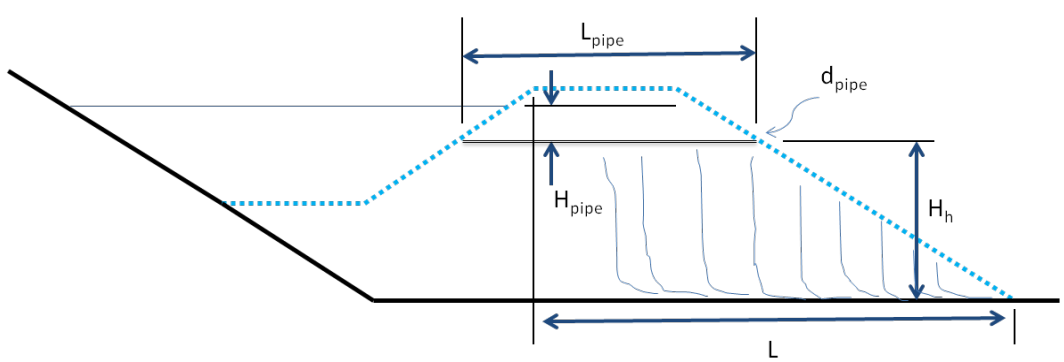

Figure 32. — Canal embankment parameters for estimating headcut advance rate due to piping flow.

The flow rate through the pipe can be estimated by applying the energy equation

$$Q = \frac{\pi\left(d_{\text{pipe}}\right)^2 \sqrt{2gH_{\text{pipe}}}}{4\sqrt{1 + f\dfrac{L_{\text{pipe}}}{d_{\text{pipe}}}}} \tag{8}$$

Assuming a relatively rough interior for the pipe, a value of Darcy's f=0.05 may be used. The unit discharge effective in advancing the headcut can then be estimated by converting the flow through the round pipe into flow of an equivalent square jet, $q = (\pi/4)^{1/2}\,(Q/d_{\text{pipe}}) = 0.886Q/\,d_{\text{pipe}}$. The time required for headcut advance is then computed as before

$$t_{\text{initiation}} = \frac{L}{\left(0.44k_d\right)\left(0.886QH_h / d_{\text{pipe}}\right)^{1/3}} \tag{9}$$

Note that the distance L is shown in Figure 32 as the distance to the upstream crest, not the full distance to the upstream end of the pipe. This leads to a shorter, more conservative estimate of the breach initiation time and is consistent with the observed behavior of the test embankments, which seemed to experience collapse of the bridge over the pipe at about the time that headcutting reached the upstream side of the crest.

Breach Initiation by Pipe Enlargement

As previously noted, the model for pipe enlargement is extremely sensitive to the values of k_d and τ_c as well as the choice of a starting condition for the piping erosion analysis. In erosion resistant materials, the model may predict a very long time to reach breach initiation, and headcut advance due to the piping flow will probably breach the embankment much more quickly. In very weak materials, this model may predict a very rapid breach, but it is likely that the headcut advance model would also predict a very rapid breach. This model is presented here primarily for its potential value in further research. The model for headcut advance due to piping is recommended for practical use at this time.

To analyze pipe enlargement, a starting diameter for the pipe must be selected. As discussed in the previous section, this should be a practical value relating to the size of piping defect that might prompt notice of the piping condition by project personnel and begin the cycle of potential operational responses to a canal emergency. With the pipe diameter and its length specified, the initial flow rate through the pipe, Q_0, can be estimated with Eq. 8, as before. The initial shear stress through the pipe can be estimated as $\tau_0 = \gamma_w S d_{\text{pipe}}/4$, with S being the hydraulic gradient acting on the pipe. The erosion time scale can then be estimated from Eq. 4, using a k_d value obtained from a hole erosion test, or a k_d value obtained from a submerged jet test and reduced by a factor of 10. The critical shear stress, τ_c, should be obtained from a hole erosion test, or the result from a jet test may be used if increased by a factor of 100. Although τ_c values for

many weak materials are believed to be practically zero for use in many erosion modeling equations, a non-zero value should be considered for this analysis. For this purpose, Table 9 (a modified version of Table 8) is suggested. Eq. 3 may be solved for the time *t* at which the dimensionless discharge reaches a pre-determined value:

$$t = t_{er} \ln\left(1 + \frac{\left(Q(t)/Q_0\right)^{2/5} - 1}{1 - \tau_c / \tau_0}\right) \tag{10}$$

Table 9. — Approximate values of τ_c in Pa as a function of compaction conditions and %clay (modified from Hanson et al. 2010). These values of τ_c are representative of submerged jet test results. For use in the piping erosion model (Eq. 10), they should be increased by a factor of 100. [1 Pa = 0.0209 psf]

% Clay (<0.002 mm)	Modified Compaction (56,250 ft-lb/ft^3)		Standard Compaction (12,375 ft-lb/ft^3)		Low Compaction (2,475 ft-lb/ft^3)	
	≥Opt WC%	<Opt WC%	≥Opt WC%	<Opt WC%	≥Opt WC%	<Opt WC%
	Critical shear stress, τ_c, Pa					
>25	16	0.16	4	0.04	1	0.01
14-25	1.6×10^{-1}	1.6×10^{-3}	4×10^{-2}	4×10^{-4}	1×10^{-2}	1×10^{-4}
8-13	1.6×10^{-3}	1.6×10^{-5}	4×10^{-4}	4×10^{-6}	1×10^{-4}	1×10^{-6}
0-7	1.6×10^{-5}	1.0×10^{-6}	4×10^{-6}	2.5×10^{-7}	1×10^{-6}	6×10^{-8}

A suggested condition defining the end of breach initiation and a transition to the breach development phase is discharge through the piping hole, $Q(t)$ equal to 5% of the normal canal discharge. The elapsed time required will be found to be relatively insensitive to the specific percentage of canal flow selected, as the discharge through the piping hole increases rapidly near the end of the breach initiation process. Eq. 10 will only be valid for $\tau_c<\tau_0$ and $Q(t)>Q_0$.

Breach Development

The breach development phase is characterized by continued headcut advancement through the upstream (canal side) slope of the embankment down to its toe, followed by widening of the breach in both directions until the breach becomes wide enough that it is no longer the hydraulic control. At this point, hydraulic control of the flow shifts to the critical-flow sections that will exist in the upstream and downstream canals. For purposes of this appraisal-level model, the period of headcut advance into the canal is assumed to be short compared to the time for breach widening, or can be incorporated into the estimate of the widening time, assuming that widening begins from a breach width of zero. The breach will be assumed to have vertical sidewalls during the widening phase and a rectangular cross-section, as observed in the physical model tests.

To estimate the breach development time, it will be necessary to first define the ending condition for this phase. We need to determine the maximum theoretical

flow that can be provided to the breach site by the upstream and downstream canals. This is accomplished by iteratively solving a system of three equations applying to critical flow (Clemmens et al. 2001):

$$Q = \sqrt{\frac{gA_c^3}{T_c}} \tag{11}$$

$$y_c = H_1 - \frac{A_c}{2T_c} \tag{12}$$

$$H_1 = h_1 + \frac{Q^2}{2gA_1^2} \tag{13}$$

For the design normal-depth flow condition of the canal, the flow depth h_1 is known and a value of H_1 can be computed using Eq. 13. Next, assume a starting value for critical depth, y_c, such as y_c=0.7H_1. For this critical depth, the cross-sectional area, A_c, and top width, T_c, of the canal may be computed. The critical discharge can then be computed from Eq. 11 and a refined estimate of y_c computed with Eq. 12. We want to keep H_1 constant, so the iteration between Eqs. 11 and 12 is continued until convergence is obtained. The maximum theoretical breach outflow, $Q_{c,max}$, will then be two times the critical discharge computed with Eq. (11), assuming that both canals have the same cross section. The critical flow depth through the rectangular breach opening will then be estimated as (2/3)y_n, where y_n is the normal depth of flow in the canal. For a rectangular channel, the critical flow depth is y_c=$(q^2/g)^{1/3}$, so the unit discharge at the end of breach widening is q=$([2y_n/3]^3 g)^{1/2}$ and the final width of the breach is

$$b_{\max} = \frac{Q_{c,\max}}{\sqrt{\left(\frac{2y_n}{3}\right)^3 g}} \tag{14}$$

Once this final width is known, the time required for breach widening can be estimated as

$$t_{\mathrm{f}} = \frac{b_{\max}}{2k_d\left(\tau_{ew} - \tau_c\right)} = \frac{b_{\max}}{2k_d[0.7\gamma_w g(y_c^{1/3} n/1.49)^2 - \tau_c]} \tag{15}$$

taking n to be 0.020 within the breach opening, as was assumed by Hunt et al. (2005). If desired, the critical shear stress, τ_c, may be assumed to be zero (i.e., use Table 8 instead of Table 9) to obtain a conservatively shorter estimate of the breach widening time.

Once the breach widening time is estimated, the peak discharge can be determined by applying Eq. 16

$$Q_{\text{peak}} = Q_{c,\max}(Q^*_{\text{peak}}) = Q_{c,\max}\frac{1.9}{(t^*_{\text{f}})^{1/6}}\left[1-\frac{1}{(L^*_{\text{ds}})^{1/3}}\right] \tag{16}$$

where t^*_{f} is the dimensionless breach development time (breach widening time) divided by the time scale reference, $t_{\text{ref}}=(D/g)^{0.5}$, and L^*_{ds} is the downstream canal reach length nondimensionalized by the hydraulic radius, L_{ds}/R_h. The peak discharge can be assumed to occur at the end of the breach widening phase. The duration of the recession curve to a flow rate of $0.5(Q_{\text{peak}}+Q_{\text{normal}})$ can then be estimated with Eq. 17.

$$t_{\text{recession}} = \frac{123}{t^{*0.66}_{\text{f}}}t_{\text{f}} \tag{17}$$

Conclusions

The research described in this report has addressed a broad array of issues related to the modeling of potential canal embankment breaches and determination of breach outflow hydrographs. Physical model tests addressed a variety of failure initiation conditions and demonstrated the influence of wide variations in erodibility of embankment soils. Erosion rates were related to applied hydraulic stresses and the erosion resistance of embankment materials as quantified with submerged jet erosion tests, tests which can be performed in the laboratory or in the field on embankments of future interest. Relations for predicting erosion rates were consistent with the work of other investigators and thus provide a basis for developing practical methods for estimating breach parameters. Equations were developed for estimating breach width and time of breach formation, with breach side slopes assumed to be vertical.

Breach outflow rates measured in the physical model tests could not reflect the effect of finite-length canal reaches with limited volumes of water to be discharged through a breach, nor could they reflect the effects of potential operational responses that might also limit the volume of water available to cause a large peak breach outflow. Numerical studies with unsteady-flow HEC-RAS models were used to quantify the effects of canal hydrodynamics. This work developed empirical equations for estimating peak breach outflow as a function of canal cross section and reach properties and breach time parameters. Combining the results of all of these efforts produced a tool for making appraisal-level estimates of breach initiation time, breach development time, peak breach outflow, and outflow hydrograph shape.

The primary factors affecting the peak breach outflow rate and the time to reach the peak outflow is the rate at which the breach develops, which is dependent on the soil erodibility and the failure initiation condition and the associated hydraulic

stresses applied to the soil. Failure mode also affects the likelihood for a breach to be discovered while in progress, early enough that an effective operational response and emergency evacuation of populations at risk are still possible. The greatest risks are associated with highly erodible embankments experiencing overtopping flow or piping under significant head. Erosion of these embankments will progress through the breach initiation phase quickly and produce a rapid breach development that causes a large peak outflow with a short time available for operational response, warning, or evacuation. Highly erodible embankments experiencing low-head piping can also be a serious threat, but may experience a slower breach initiation due to the low stresses associated with piping under a low hydraulic gradient. If breach initiation can be detected at an early stage, there may be time for intervention to shut down the canal, prevent the breach, or carry out effective warning and evacuation actions. However, if such a breach is not detected in progress, a rapid breach development and large peak outflow are likely when the embankment reaches the threshold for complete failure.

The procedures developed in this report for making appraisal-level estimates of breach outflow hydrographs have been developed from analysis of a small population of canal configurations, and thus should be tested against data obtained from real canal failures or from additional numerical simulations. The development of a canal-specific breach model or the incorporation of canal-specific features into existing dam breach models would be valuable for the detailed simulation of potential failures of canals in urban environments, where populations at risk are large and greater accuracy may be valuable.

References

ASTM, 2003. Annual Book of ASTM Standards, Section 4: Construction, Vol. 04.08. Philadelphia, Pa.: ASTM.

Bonelli, S., and Brivois, O., 2007. The scaling law in the hole erosion test with a constant pressure drop. *International Journal for Numerical and Analytical Methods in Geomechanics*, 24 pp. Wiley InterScience (www.interscience.wiley.com). DOI: 10.1002/nag.683

Bonelli, S., O. Brivois, R. Borghi, and N. Benahmed. 2006. On the modelling of piping erosion. *Comptes Rendus Mecanique* 334, Elsevier SAS, pp. 555-559.

Bridgewater Canal Company, Ltd. 2011. Breach of the Bridgewater Canal into the River Bollin at Dunham 1971. http://www.bridgewatercanal.co.uk/timeline12.html

Chow, V.T., 1959. *Open-Channel Hydraulics*, McGraw-Hill, Inc., New York, 534-536.

Clemmens, Albert J., Tony L. Wahl, Marinus G. Bos, and John A. Replogle, 2001, *Water Measurement with Flumes and Weirs*, ILRI Publication 58, International Institute for Land Reclamation and Improvement, Wageningen, The Netherlands, p. 224.

Dun, R.W.A., 2007. An improved understanding of canal hydraulics and flood risk from breach failures. *Water and Environment Journal.* 21(1): 9-18.

Erdogan, Z., and T.L. Wahl, 2008. Results of laboratory physical properties and hole erosion tests, Truckee Canal Embankment Breach, Newlands Project, Nevada. Technical Memorandum No. MERL-08-6, U.S. Dept. of the Interior, Bureau of Reclamation, Denver, CO.

Hanson, G. J., K. M. Robinson, K. R. Cook. 2001. Prediction of headcut migration using a deterministic approach. *Transactions of the ASAE*. 44(3):525-531.

Hanson, G.J., and Cook, K.R., 2004. Apparatus, test procedures, and analytical methods to measure soil erodibility *in situ*. *Applied Engineering in Agriculture*, 20(4):455-462.

Hanson, G.J., Cook, K.R., and Hunt, S.L., 2005. Physical modeling of overtopping erosion and breach formation of cohesive embankments. *Transactions of the ASAE*, 48(5): 1783−1794.

Hanson, G.J., and Hunt, S.L., 2007. Lessons learned using laboratory jet method to measure soil erodibility of compacted soils. *Applied Engineering in Agriculture*, 23(3):305-312.

Hanson, Gregory J., Wahl, Tony L., Temple, Darrel M., Hunt, Sherry L., and Tejral, Ronald D., 2010. Erodibility characteristics of embankment materials. In: *Dam Safety 2010*. Proceedings of the Association of State Dam Safety Officials Annual Conference, September 19-23, 2010, Seattle, WA. (CDROM).

Hanson, G.J., Tejral, R.D., Hunt, S.L., Temple, D.M., 2010. Internal erosion and impact of erosion resistance. Proceedings of the United States Society on Dams, 30th Annual Conference, Sacramento, CA April 12-16, 2010.

Hanson, G.J., Temple, D.M., Hunt, S.L., and Tejral R.D., 2011. Development and characterization of soil material parameters for embankment breach. *Applied Engineering in Agriculture* (accepted for publication on March 22, 2011).

Hunt, S.L., Hanson, G.J., Cook, K.R., and Kadavy, K.C., 2005. Breach widening observations from earthen embankment tests. *Transactions of the ASAE*, 48(3):1115-1120.

Hydrologic Engineering Center, 2010. CPD-68. HEC-RAS River Analysis System, User's Manual, Version 4.1, January 2010. U.S. Army Corps of Engineers, Davis, CA.

Hydrologic Engineering Center, 2010. CPD-69. HEC-RAS River Analysis System, Hydraulic Reference Manual, Version 4.1, January 2010. U.S. Army Corps of Engineers, Davis, CA.

McKulla, M., 2008. Truckee Canal breach station 714+00 geologic investigations. U.S. Dept. of the Interior, Bureau of Reclamation, Mid-Pacific Region, Geology Branch (MP-230), March 2008.

Mohamed, M.A.A., 2002. Embankment breach formation and modelling methods. Ph. D. thesis. Open University, UK.

Pierce, M.W., Thornton, C.I., and Abt, S.R., 2010. Predicting peak outflow from breached embankment dams. *Journal of Hydrologic Engineering*, 15(5):338-349.

Powers, K. (2005). Aging Infrastructure: Dam Safety. Congressional Research Service, September 29, 2005. http://digital.library.unt.edu/govdocs/crs/permalink/meta-crs-7622:1

Russell, K., and Bountry, J., 2008. Hydraulic model results for Truckee Canal breach evaluation. U.S. Dept. of the Interior, Bureau of Reclamation, Sedimentation and River Hydraulics Group, Denver, CO.

Temple, D.M., Hanson, G.J., Nielsen, M.L., and Cook, K., 2005. Simplified breach analysis model for homogeneous embankments: Part 1, Background and model components. USSD Technologies to Enhance Dam Safety and the Environment, 25th Annual USSD Conference, Salt Lake City, Utah.

Temple, D.M., Hanson, G.J., and Nielsen, M.L., 2006. WINDAM – Analysis of overtopped earth embankment dams. ASABE Annual International Meeting, Portland, OR, 9 - 12 July 2006.

URS, 2008. Truckee Canal failure on 5 January 2008: investigative evaluation report. Prepared for U.S. Department of the Interior, Bureau of Reclamation, Mid-Pacific Region, Sacramento, CA, Contract 06CS204097A. March 2008.

USBR, 1990. *Earth Manual, Part 2*, 3rd ed. U.S. Dept. of the Interior, Bureau of Reclamation, Materials Engineering Research Laboratory, Denver, CO.

Wahl, Tony L., 1998, *Prediction of Embankment Dam Breach Parameters: A Literature Review and Needs Assessment*, Dam Safety Research Report DSO-98-004, U.S. Dept. of the Interior, Bureau of Reclamation, Denver, Colorado, July 1998.

Wahl, Tony L., 2004. Uncertainty of predictions of embankment dam breach parameters. *Journal of Hydraulic Engineering*, 130(5):389-397.

Wahl, Tony L., 2007. "Laboratory Investigations of Embankment Dam Erosion and Breach Processes", CEA Technologies Inc., Dam Safety Interest Group, CEATI Report No. T032700-0207A, 60 pp.

Wahl, Tony L., Regazzoni, Pierre-Louis, and Erdogan, Zeynep, 2008. *Determining Erosion Indices of Cohesive Soils with the Hole Erosion Test and Jet Erosion Test*, Dam Safety Technology Development Report DSO-08-05, U.S. Dept. of the Interior, Bureau of Reclamation, Denver, Colorado, 45 pp.

Wahl, Tony L., 2009. "Evaluation of New Models for Simulating Embankment Dam Breach," Dam Safety '09, Annual Meeting of the Association of State Dam Safety Officials (ASDSO), Sept. 27-Oct. 1, 2009, Hollywood, FL.

Wahl, Tony L., 2010. Dam breach modeling – an overview of analysis methods. Joint Federal Interagency Conference on Sedimentation and Hydrologic Modeling, Las Vegas, NV, June 27-July 1, 2010.

Xu, Y. and Zhang, L.M., 2009. Breaching parameters for earth and rockfill dams, *Journal of Geotechnical and Geoenvironmental Engineering*, 135(12):1957-1970.